ANALYSIS OF OZONE PRODUCTION AND ITS SENSITIVITY IN HOUSTON USING THE DATA COLLECTED DURING DISCOVER-AQ

AQRP PROJECT 14-020

FINAL REPORT (VER 3.0)

SUBMITTED TO

UNIVERSITY OF TEXAS - AUSTIN
AIR QUALITY RESEARCH PROGRAM (AQRP)

AND

TEXAS COMMISSION ON ENVIRONMENTAL QUALITY (TCEQ)

BY:

XINRONG REN
UNIVERSITY OF MARYLAND
DEPARTMENT OF ATMOSPHERIC AND OCEANIC SCIENCE
COLLEGE PARK, MD

QAPP Category Number: III

Type of Project: Data Analysis & Research Model Application

QA Requirements:
Audits of Data Quality: Cat III = 10% Required

NOVEMBER 10, 2015

EXECUTIVE SUMMARY

Understanding the non-linear relationship between ozone (O_3) production and its precursors is critical for the development of an effective ozone control strategy. Despite great efforts undertaken in the past decades to address the problem of high ozone concentrations, our understanding of the key precursors that control tropospheric ozone production remains incomplete and uncertain. Sensitivity of ozone production to nitrogen oxides (NO_x) and volatile organic compounds (VOCs) represents a major uncertainty for oxidant photochemistry in urban areas and is expected to vary from location to location and at different times of the day.

The Deriving Information on Surface Conditions from COlumn and VERtically Resolved Observations Relevant to Air Quality (DISCOVER-AQ) campaign in Houston in August/September 2013 provided rich data sets to examine and improve our understanding of atmospheric photochemical oxidation processes related to the formation of secondary air pollutants like ozone and particulate matter (PM). In this project, an analysis of ozone production and its sensitivity to NO_x and VOCs is conducted. An observation-constrained box model based on the Carbon Bond mechanism, Version 5 (CB05), was used to study the photochemical processes along the NASA P-3B flight track as well as at eight surface sites where the P-3B conducted spiral profiles. Ozone production rates were calculated at different locations and at different times of day and its sensitivity to NO_x and VOCs were investigated. Ozone production efficiency (OPE), defined as the ratio of the ozone production rate to the NOx oxidation rate, was calculated using observations as well as box and CMAQ model results and its correlation with other parameters such as radical sources and NOx mixing ratio was evaluated.

The purpose of this work is to provide scientific information for policy decisions related to ozone control strategies for the State Implementation Plan (SIP) in Texas. This project specifically addresses one of the AQRP priority research areas: Improving the understanding of ozone and particulate matter (PM) formation, and quantifying the characteristics of emissions in Texas through analysis of data collected during the DISCOVER-AQ campaign. The following tasks were performed in this project and results from each task are lasted:

(1) *To investigate spatial variations of ozone production and its sensitivity to NO_x and VOCs in Houston during DISCOVER-AQ.*

Hotspots of ozone production, $P(O_3)$, over Downtown Houston and the Houston Ship Channel were observed due to significant emission sources in this area. Diurnal variations of ozone production rate at eight individual locations where the P-3B conducted vertical spirals show that the ozone production rate is on average more than 10 ppbv hr^{-1} at locations with high NOx and VOC emissions such as Deer Park, Moody Tower and Channelview, while at locations away from the urban center with lower emissions of ozone precursors such as Galveston, Smith Point, and Conroe, the ozone production rate is usually less than 10 ppbv hr^{-1} on average.

(2) *To investigate temporal variations of ozone production and its sensitivity to NO_x and VOCs in Houston during DISCOVER-AQ.*

On average ozone production, $P(O_3)$, was about 20-30 ppbv hr^{-1} in the morning and 5-10 ppbv hr^{-1} in the afternoon during DISCOVER-AQ in Houston in 2013. The diurnal variation of $P(O_3)$ shows a broad peak in the morning with significant $P(O_3)$ in the afternoon obtained on ten flight days in September 2013. It is noticed that high $P(O_3)$ mainly occurred with L_N/Q, where

L_N is the radical loss via the reactions with NOx and Q is the total primary radical production, is greater than 0.5, i.e., in the VOC sensitive regime.

Ozone production tended to be more VOC sensitive in the morning with high $P(O_3)$ of 30-50 ppbv hr^{-1}. The diurnal variation of L_N/Q indicates that $P(O_3)$ was mainly VOC sensitive in the early morning and then transited towards the NOx sensitive regime later in the day. High $P(O_3)$ in the morning was mainly associated with VOC sensitivity due to high NOx levels in the morning. Ozone production was generally NOx sensitive in the afternoon with spatial variations, even though there were periods when $P(O_3)$ was VOC sensitive. At Deer Park, $P(O_3)$ was mostly VOC sensitive for the entire day.

(3) To provide scientific information for a non-uniform emission reduction strategy to control O_3 pollution in Houston using spatial and temporal variations of ozone production and its sensitivity to NO_x and VOCs.

Based on the results from this project, a non-uniform emission reduction strategy, i.e., where/when to control what, for an O_3 pollution control plan in Houston was derived to provide scientific information for policy decisions. In general, O_3 production tends to be more VOC sensitive in the morning with high ozone production rates. The diurnal variation of L_N/Q indicates that $P(O_3)$ was mainly VOC sensitive in the early morning and then transited towards the NOx sensitive regime later in the day. High $P(O_3)$ in the morning was mainly associated with VOC sensitivity due to high NOx levels in the morning. This suggests that control of VOC may be an effective way to control O_3 in Houston. In the afternoon, O_3 production is more NOx sensitive with spatial variabilities. At Deer Park, ozone production was mostly VOC sensitive for the entire day. At Moody Tower and Channelview, ozone production was VOC sensitive or in the transition regime. At Smith Point and Conroe, ozone production was mostly NOx sensitive for the entire day.

(4) To calculate ozone production efficiency (OPE) at different locations using the number of ozone molecules produced per molecule of NOx consumed in the box and CMAQ models.

Ozone production efficiency (OPE) was about 8 during DISCOVER-AQ 2013 in Houston, i.e., 8 molecules of ozone were produced when one molecule of NOx was consumed. This OPE value is greater than the average OPE value (5.9±1.2) obtained during the Texas Air Quality Study in 2006 (TexAQS2006) [Neuman et al., 2009]. One possible reason for this increased OPE is the continuous reduction in NOx emissions in Houston between 2006 and 2013 pushed NOx levels closer to 1 ppbv in 2013, thus OPE increased since OPE increases as NOx decreases when the NOx level is greater than ~1 ppbv (Figure 2-11). This OPE value is about a factor of 1.5 to 2 higher than the OPE obtained in the DISCOVER-AQ 2011 study in Maryland due to higher photochemical reactivity in Houston.

The results from this work strengthen our understanding of O_3 production and development of the State Implementation Plan (SIP), which is essential to meet the primary and secondary National Ambient Air Quality Standards (NAAQS) for ozone.

TABLE OF CONTENTS

LIST OF FIGURES

LIST OF TABLES

Table **Page**

1. INTRODUCTION

1.1 Background

Despite great efforts undertaken in the past decades to address the problem of high ozone concentrations, our understanding of the key precursors that control tropospheric ozone production remains incomplete and uncertain [Molina and Molina, 2004; Xue et al., 2013]. The ozone problem is a complex coupling of emissions, chemical transformation, and dynamic transport at different scales [Jacob, 1999]. A major challenge in regulating ozone pollution lies in comprehending its complex and non-linear chemistry with respect to ozone precursors, i.e., nitrogen oxides (NO_x) and volatile organic compounds (VOCs) that varies with time and location (Figure 1-1). Understanding of the non-linear relationship between ozone production and its precursors is critical for the development of an effective ozone control strategy.
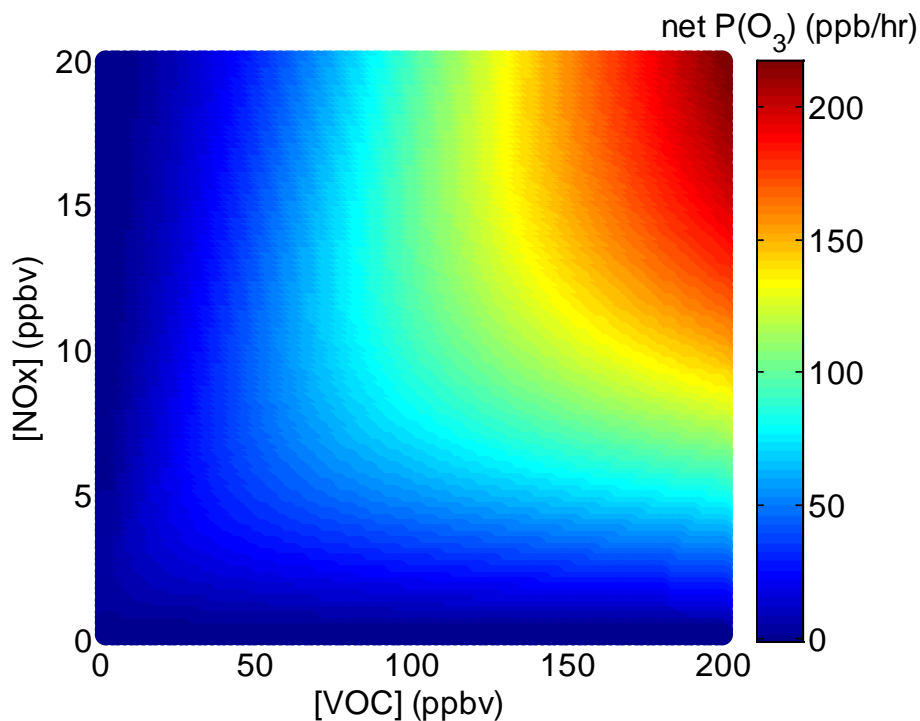
Figure 1-1. Ozone production empirical kinetic modeling approach (EKMA) diagram using a box model results with NOx levels varying from 0-20 ppbv and VOC levels from 0-200 ppbv while the mean concentrations of other species observed during DISCOVER-AQ in Houston in 2013 were used to constrain the box model which is described in Appendix C and Appendix D. This diagram clearly shows the sensitivity of ozone production to NOx and VOCs in Houston.

Sensitivity of ozone production to NO_x and VOCs represents a major uncertainty for oxidant photochemistry in urban areas [Sillman et al., 1995; 2003]. In urban environments, ozone is formed through photochemical processes when its precursors NO_x and VOCs are emitted into the atmosphere from many sources. Depending on physical and chemical conditions, the production of ozone can be either NO_x-sensitive or VOC-sensitive due to the complexity of these photochemical processes. Therefore, effective ozone control strategies heavily rely on the accurate understanding of how ozone responds to the reduction of NO_x and VOC emissions, which is usually simulated by photochemical air quality models [e.g., Sillman et al., 2003; Lei et al., 2004; Mallet and Sportisse, 2005; Li et al, 2007; Tang et al., 2010; Xue et al., 2013].

However, those model-based studies have inputs or parameters subject to large uncertainties, which can affect not only the simulated levels of ozone but also the ozone dependence on its precursors.

There are very limited observation-based studies on ozone production and its sensitivity to NO_x and VOCs. Using in-situ aircraft observations, Kleinman et al. [2005a] studied ozone production in five U.S. cities and found that ozone production rates vary from nearly zero to 155 ppb h^{-1} with differences in ozone production depending on precursor concentrations, such as radical sources, NO_x, and VOCs. They also found that in Houston, NO_x and light olefins are co-emitted from petrochemical facilities leading to the highest ozone production of the five cities [Kleinman et al., 2005a]. Using the data collected at a single location during the Study of Houston Atmospheric Radical Precursors (SHARP) in spring 2009, a temporal variation of O_3 production was observed: VOC-sensitive in the early morning and NO_x-sensitive for most of the afternoon [Ren et al., 2013]. This is similar to the behavior observed in two previous summertime studies in Houston: the Texas Air Quality Study in 2000 (TexAQS 2000) and the TexAQS II Radical and Aerosol Measurement Project in 2006 (TRAMP 2006) [Mao et al., 2010]. In a recent study using measurements in four cities in China, the ozone production was found to be in a VOC-sensitive regime in both Shanghai and Guangzhou, but in a mixed regime in Lanzhou [Xue et al., 2013]. These studies have limited spatial and/or temporal coverage in the data collected during the field campaigns. More investigation of spatial and temporal variations of ozone production and its sensitivity to NO_x and VOCs is thus needed in order to provide a scientific basis to develop a non-uniform emission reduction strategy for O_3 pollution control in urban areas like Houston.

During the Deriving Information on Surface Conditions from COlumn and VERtically Resolved Observations Relevant to Air Quality (DISCOVER-AQ) campaign in Houston in August/September 2013, a comprehensive suite of measurements were collected from various platforms including the National Aeronautics and Space Administration (NASA) P-3B and B-200 aircraft, ground surface sites, and mobile laboratories [DISCOVER-AQ whitepaper]. The rich data sets produced during this campaign provide a great opportunity to examine and improve our understanding of atmospheric photochemical oxidation processes related to the formation of secondary air pollutants like ozone and particulate matter (PM). In this project, an analysis of ozone production and its sensitivity to NO_x and VOCs using a chemical transport model and an observation-constrained box model was conducted. Spatially and temporally resolved ozone production and its sensitivity were also investigated. Based on the results from this project, a non-uniform emission reduction strategy, i.e., where and when to control certain species for an O_3 pollution control plan for Houston is proposed. This is useful in providing scientific information for policy decisions.

1.2 DISCOVER-AQ 2013 Campaign Overview

The NASA P-3B was deployed in the DISCOVER-AQ 2013 campaign in Houston. Measurements directly related to satellite observations of air quality include ozone (O_3), nitrogen dioxide (NO_2), formaldehyde (HCHO), and aerosol optical and microphysical properties. Additional critical variables needed for retrievals and data interpretation include atmospheric state (temperature, pressure, wind speed and wind direction), water vapor (H_2O), carbon monoxide (CO), methane (CH_4), carbon dioxide (CO_2), nitric oxide (NO), the components of reactive nitrogen, and aerosol inorganic and organic composition. The P-3B instruments were well characterized having been deployed previously on multiple airborne campaigns and used in published research findings. The P-3B is an ideal choice for a profiling aircraft for several

reasons: 1) it is capable of hosting a comprehensive atmospheric chemistry and aerosol payload, 2) it is ideal for profiling the lower atmosphere because it is a four-engine turboprop with heavy lift, and 3) it has sufficient flight duration (eight hours) for sampling throughout the day [DISCOVER-AQ whitepaper].

Eight surface monitoring stations were selected where the P-3B conducted vertical spirals. These monitoring stations provided in situ observations of trace gases (O_3, CO, NO, reactive nitrogen species (NOy), sulfur dioxide (SO_2)), aerosol lidar observations, and balloon soundings of ozone, NO_2, NOx and water vapor. These eight surface monitoring stations include Smith Point, Galveston, Manvel Croix, Deer Park, Channelview, Conroe, West Houston, and Moody Tower. The eight surface sites chosen for the deployment were evaluated prior to DISCOVER-AQ with regard to the presence or absence of complementary chemical and meteorological measurements which enhanced the utility of the aircraft measurement suite; the nature, strength, and likely impact of nearby point and mobile emission sources; the nature, height, and extent of nearby structures and vegetation, and their likely influence on local meteorology and wind flow patterns; and any other characteristic which might render the site physically or chemically unrepresentative of the surrounding area [DISCOVER-AQ whitepaper].

Additionally, the primary component of the surface network was the Pandora instrument, a sun-tracking UV-visible spectrometer capable of continuous monitoring of trace gas columns for O_3, NO_2, and HCHO throughout the day. Pandora has demonstrated capability, is relatively low-cost, and can be left unattended making it ideal for use in a distributed network.

1.3 Project Objectives

The purpose of this work is to provide scientific information for policy decisions related to ozone control strategies for the State Implementation Plan (SIP) in Texas, particularly those that heavily rely on the use of appropriately represented chemical models. This project specifically addresses one of the AQRP priority research areas: Improving the understanding of ozone and particulate matter (PM) formation, and quantifying the characteristics of emissions in Texas through analysis of data collected during the DISCOVER-AQ campaign [Texas Air Quality Research Program, 2013]. The following tasks were performed in this project:

(1) To investigate spatial variations of ozone production and its sensitivity to NO_x and VOCs in Houston during DISCOVER-AQ.

(2) To investigate temporal variations of ozone production and its sensitivity to NO_x and VOCs in Houston during DISCOVER-AQ.

(3) To provide scientific information for a non-uniform emission reduction strategy to control O_3 pollution in Houston using spatial and temporal variations of ozone production and its sensitivity to NO_x and VOCs.

(4) To calculate ozone production efficiency (OPE), defined as the ratio of the ozone production rate to the NOx oxidation rate, at different locations using the ratio of ozone production rate to the NO_x oxidation rate calculated in the box model.

2. DATA ANALYSIS (*BY OBJECTIVE)*

In this project, the University of Maryland data analysis team applied a photochemical model based on the CB05 chemical mechanism and a chemical transport model based on Weather Research and Forecast - Community Multi-scale Air Quality (WRF-CMAQ) to analyze the data collected in Houston during DISCOVER-AQ in 2013. Model simulations and data analysis results are summarized below. Because high ozone concentrations and production rates were observed on September 25 and 26 during the DISCOVER-AQ period, there is value in analyzing September 25 and 26 separately. Thus two sets of results – one for all flights conducted on September 4, 6, 11, 12, 13, 14 and 24 (excluding two fights on September 25 and 26) and another for the two flights on these two days September 25 and 26 – were used in the following analysis.

2.1 OBJECTIVE 1. To investigate spatial variations of ozone production and its sensitivity to NOx and VOCs in Houston during DISCOVER-AQ.

During the day, the photochemical O_3 production rate is essentially the production rate of NO_2 molecules from HO_2 (hydroperoxyl radical) + NO and RO_2 (organic peroxyl radical, where R represents a group of organic radical such as CH_3, $CH3CH_2$, …) + NO reactions [*Finlayson-Pitts and Pitts*, 2000]. The net instantaneous O_3 production rate, $P(O_3)$, can be written approximately as the following equations:

$$P = k_{NO+HO2} [NO][HO_2] + \Sigma\ \alpha_i k_{NO+RO2i} [NO][RO_{2i}], \quad \alpha_i: NO_2 \text{ yield in } RO_{2i}+ NO \quad (1)$$

$$L = k_{OH+NO2+M} [OH][NO_2][M] + k_{O(1D)+H2O}[O(^1D)][H_2O] + k_{HO2+O3} [O_3][HO_2]$$

$$+ k_{OH+O3}[O_3][OH] + \Sigma\ k_{O3+VOCi} [O_3][VOC_i] \quad (2)$$

$$P(O_3): P(O_3)_{net} = P - L \quad (3)$$

where, *k term*s are the reaction rate coefficients. The terms in Eq. (2) correspond to the reaction of OH and NO_2 to form nitric acid, the formation of organic nitrates, $P(RONO_2)$, the reactions of OH and HO_2 with O_3, the photolysis of O_3 followed by the reaction of $O(^1D)$ with H_2O, and O_3 reactions with alkenes.

Figure 2-1 shows net ozone production rate, $P(O_3)$, calculated using the box model (described in Appendix C and Appendix D) results along the P-3B flight track. There are several $P(O_3)$ hotspots over the Houston Ship Channel as well as downwind over Galveston Bay. This is expected because of large emissions of ozone precursors (NOx and VOC) from the Houston Ship Channel. The highest $P(O_3)$ up to ~140 ppbv hr^{-1} were observed over Houston Ship Channel. High $P(O_3)$ up to ~80-90 ppbv hr^{-1} were observed over Galveston Bay, mainly on September 25, 2013, consistent with high ozone levels observed across the Houston area on that day. Comparing to the other flights, the two flights on September 25 and 26 had similar ozone production rates beyond the Houston Ship Channel and its downwind area over the Galveston Bay.
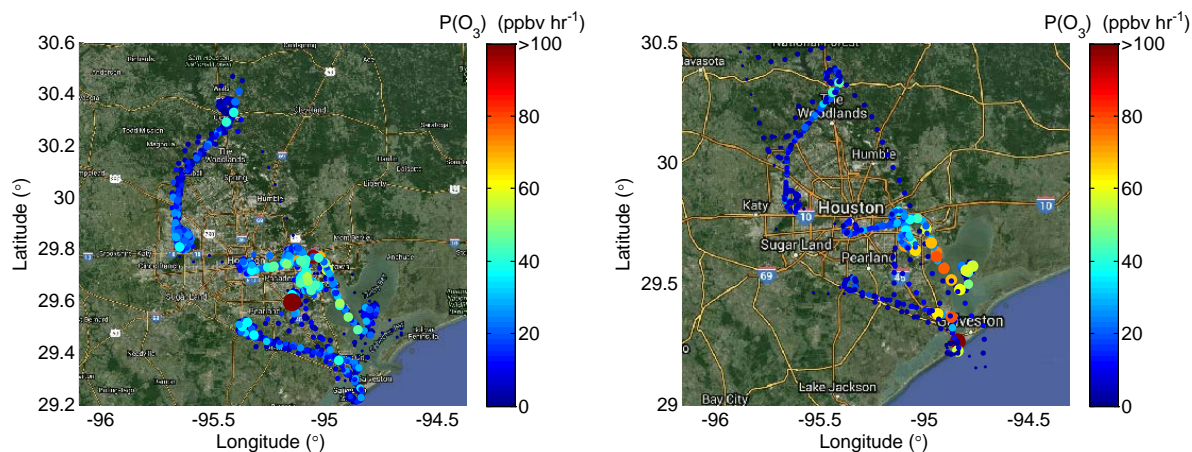
Figure 2-1. Net ozone production rate, P(O₃) calculated using the box model results along the P-3B flight track during DISCOVER-AQ in Houston in 2013 for all flights except two flights on September 25 and 26 (*left*) and for two flights on September 25 and 26 (***Right***). The size of dots is proportional to P(O₃).

The dependence of O_3 production on NOx and VOCs can be categorized into two typical scenarios: NO_x sensitive and VOC sensitive. In this work, the method proposed by *Kleinman* [2005b] is used to evaluate the O_3 production sensitivity. In this method, ozone production is a function of NOx and VOCs. The sensitivity of ozone production can be determined by an indicator L_N/Q, where L_N is the radical loss via the reactions with NO_x and Q is the total primary radical production. Because the radical production rate is approximately equal to the radical loss rate, this L_N/Q ratio represents the fraction of radical loss due to NO_x. It was found that when L_N/Q is significantly less than 0.5, the atmosphere is in a NO_x-sensitive regime, and when L_N/Q is significantly greater than 0.5, the atmosphere is in a VOC-sensitive regime [*Kleinman et al.*, 2001; *Kleinman*, 2005b]. Note that the contribution of organic nitrates impacts the cut-off value for L_N/Q to determine the ozone production sensitivity to NO_x or VOCs and this value may vary slightly around 0.5 in different environments.

Figure 2-2 shows the indicator L_N/Q of ozone production sensitivity along the P-3B flight track for all flights on September 4, 6, 11, 12, 13, 14, 24 (left plot) and two flights on September 25 and 26. P(O₃) was mainly VOC-sensitive over the Houston Ship Channel and its surrounding urban areas due to large NOx emissions. This is the case for all flights including the ones conducted on September 25 and 26. Over the areas away from the center of the city with relatively low NOx emissions, P(O₃) was usually NOx-sensitive. For other flights but the two flights on September 25 and 26, there were period when P(O₃) was mainly VOC-sensitive (i.e., $L_N/Q>0.5$) in the areas to the northwest and southwest of the Houston Ship Channel. This mainly occurred this morning periods during the flights when NOx concentrations were high.
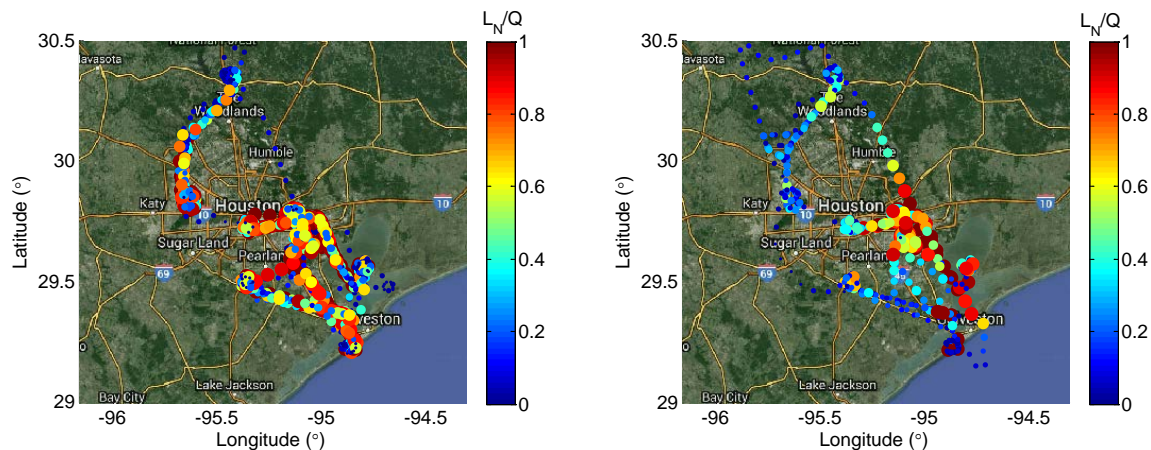
Figure 2-2. Ozone production sensitivity indicator, L_N/Q, along the P-3B flight track during DISCOVER-AQ in Houston in 2013 for all flights except two flights on September 25 and 26 (*left*) and for two flights on September 25 and 26 (***Right***). $P(O_3)$ is VOC-sensitive when $L_N/Q > 0.5$, and NOx-sensitive when $L_N/Q < 0.5$.

Vertical profiles of ozone production rate ($P(O_3)$), ozone loss rate ($L(O_3)$), and net ozone production calculated using the box model results show that (1) $RO_2 + NO$ makes about the same amount of O_3 as $HO_2 + NO$ in the model; (2) O_3 photolysis followed by $O(^1D)+H_2O$ is a dominant process for the photochemical ozone loss; and (3) the maximum net $P(O_3)$ appeared near the surface below 1 km (Figure 2-3). For the two flights on September 25 and 26, even though the highest ozone production rate was obtained near the Houston Ship Channel and its downwind area at certain time, the average ozone production rate on September 25 and 26 is not significantly different from those observed on other flight days (Figure 2-3).
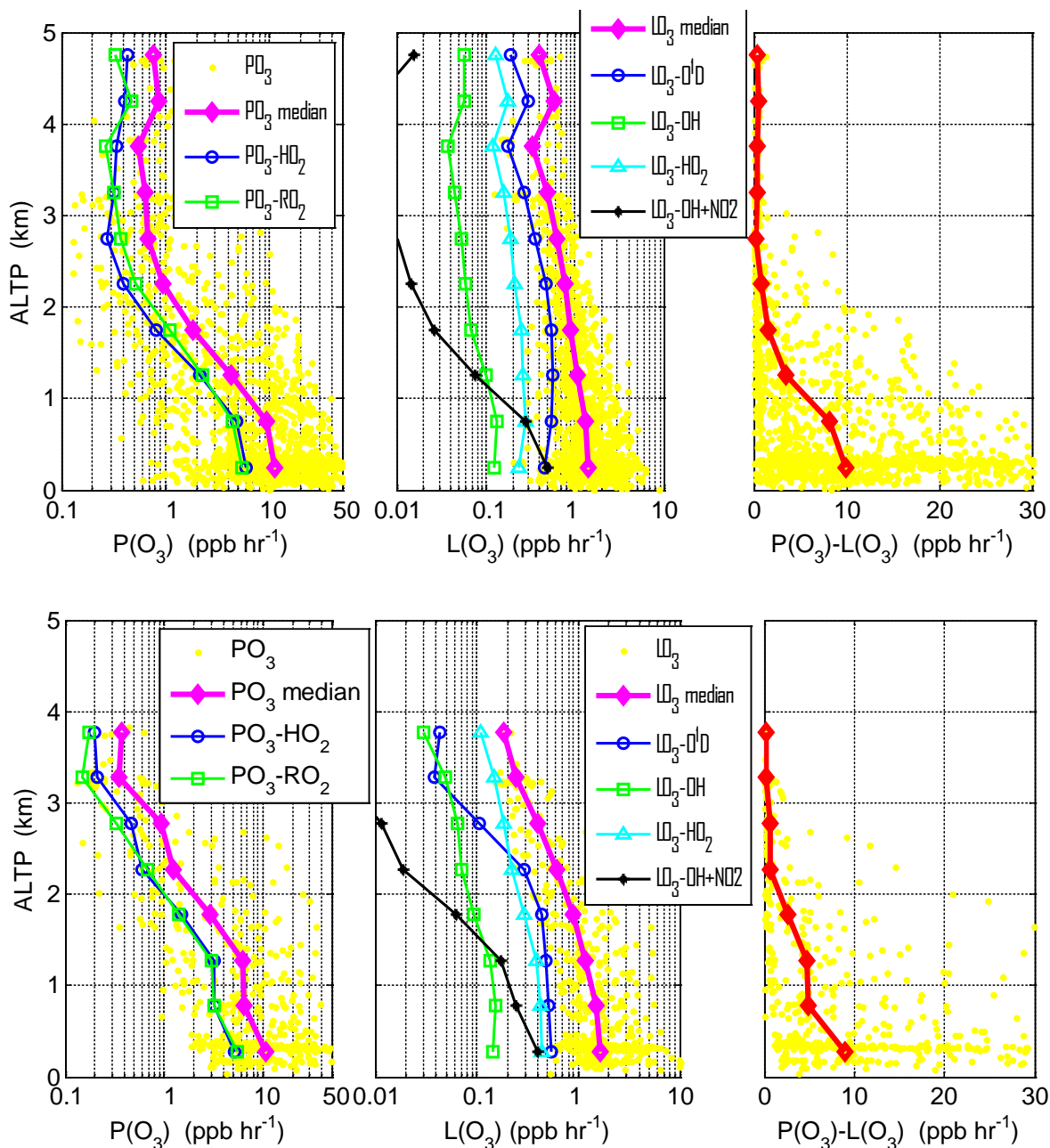
Figure 2-3. Vertical profiles of ozone production rate (left), ozone loss rate (middle), and net ozone production rate (right) during DISCOVER-AQ in Houston in 2013 for all flights except two flights on September 25 and 26 (***top*** 3 plots) and for two flights on September 25 and 26 (***bottom*** 3 plots).

2.2 OBJECTIVE 2. To investigate temporal variations of ozone production and its sensitivity to NOx and VOCs in Houston during DISCOVER-AQ.

In the diurnal variations of $P(O_3)$, a broad $P(O_3)$ peak in the morning with significant $P(O_3)$ in the afternoon was obtained on ten flight days during DISCOVER-AQ in Houston in 2013 (Figure 2-4). It is noticed that high $P(O_3)$ mainly occurred with $L_N/Q > 0.5$ (i.e., in the

VOC sensitive regime). For the two flights on September 25 and 26, the ozone production rates in the morning are higher than that for other flights, but in the afternoon the average ozone production rate on September 25 and 26 is more or less the same as those observed on other flight days (Figure 2-4).
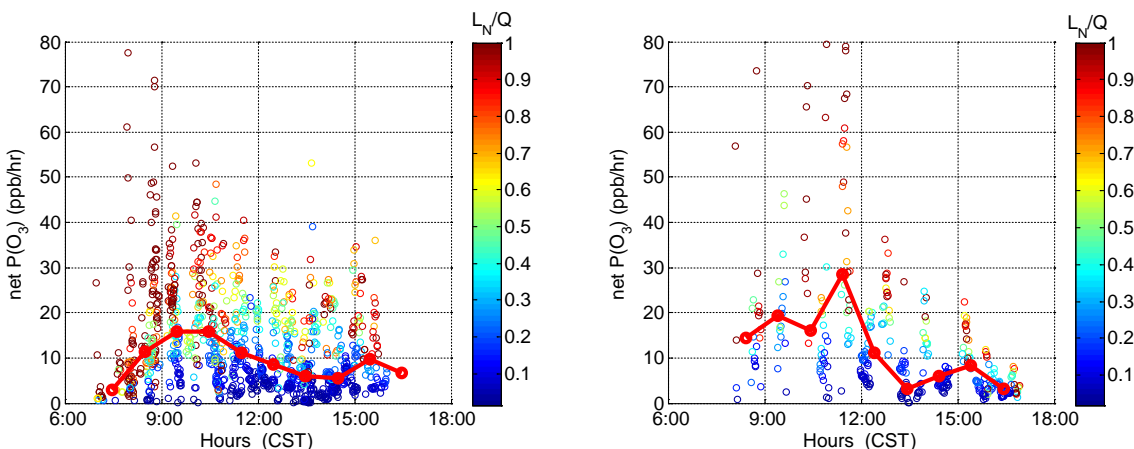
Figure 2-4. Diurnal variation of ozone production rate colored with the indicator L_N/Q on ten flight days during DISCOVER-AQ in Houston in 2013 for all flights except two flights on September 25 and 26 (*left*) and for two flights on September 25 and 26 (***Right***). The solid red circles represent the median values in hourly bins of $P(O_3)$. Data are limited with the pressure altitude less than 1000 m to represent the lowest layer of the atmosphere.

The diurnal variation of L_N/Q indicates that $P(O_3)$ was mainly VOC sensitive in the early morning and then transited towards the NOx sensitive regime later in the day for the flight other than September 25 and 26 (Figure 2-5, left plot). For the two flights on September 25 and 26, the diurnal variation of L_N/Q indicates that $P(O_3)$ was NOx sensitive for the entire day. In both case, high $P(O_3)$ in the morning was mainly associated with VOC sensitivity due to high NOx levels in the morning (points in the cycles in Figure 2-5). Even though $P(O_3)$ was mainly NOx sensitive in the afternoon between 12:00 and 17:00 (CST), there were periods when $P(O_3)$ was VOC sensitive, e.g., the hot color points above the red line in Figure 2-4.
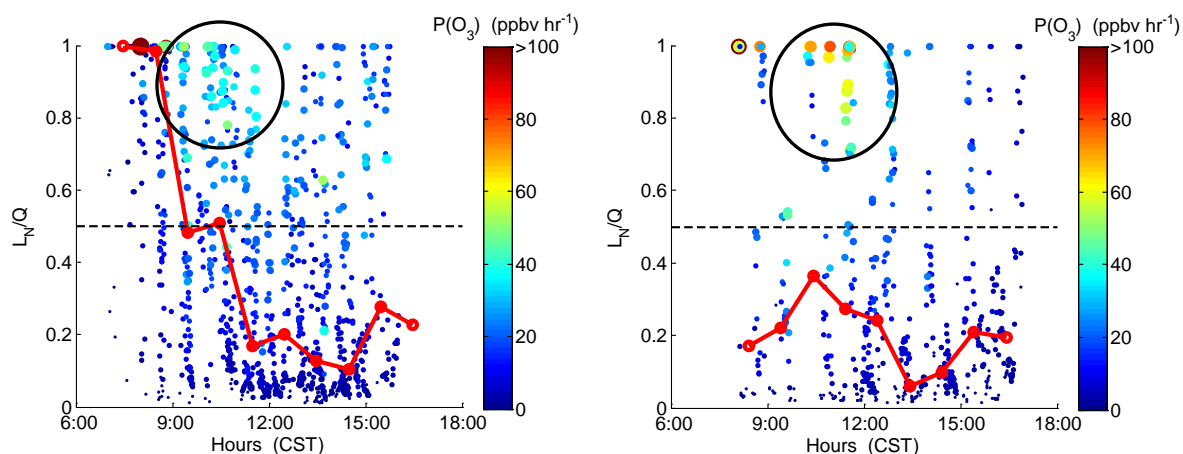
Figure 2-5. Diurnal variation of the indicator L_N/Q of ozone production rate sensitivity colored with ozone production rate below 1000 m during DISCOVER-AQ in Houston in 2013 for all

flights except two flights on September 25 and 26 (*left*) and for two flights on September 25 and 26 (***Right***). The linked red circles are the median values in hourly bins of L_N/Q. The dashed lines represent $L_N/Q = 0.5$. $P(O_3)$ is VOC-sensitive when $L_N/Q > 0.5$, and NOx-sensitive when $L_N/Q < 0.5$.

2.3 OBJECTIVE 3. To provide scientific information for a non-uniform emission reduction strategy to control O_3 pollution in Houston using spatial and temporal variations of ozone production and its sensitivity to NOx and VOCs.

Diurnal variations of ozone production rate at eight individual locations where the P-3B conducted vertical spirals show that the ozone production is greater than 10 ppb hr^{-1} on average at locations with high NOx and VOC emissions such as Deer Park, Moody Tower and Channelview, while at locations away from the urban center with lower emissions such as Galveston, Smith Point, and Conroe, the ozone production is usually less than 10 ppb hr^{-1} on average (Figure 2-6).
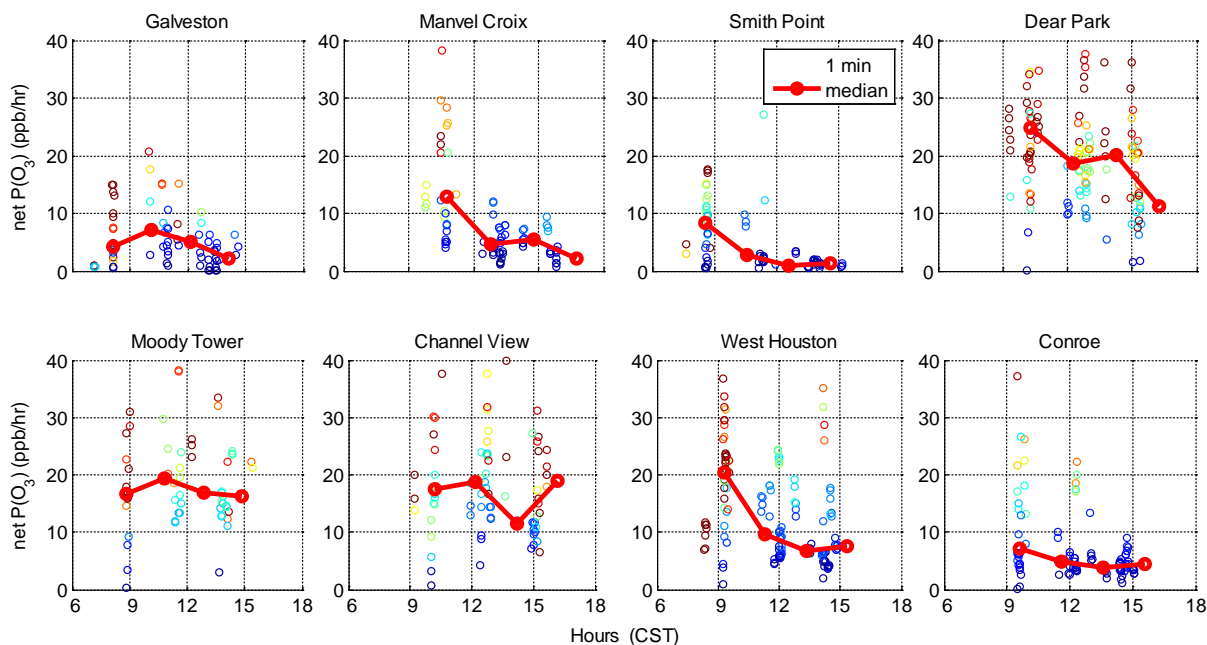
Figure 2-6. Diurnal variations of ozone production rate at eight individual spiral locations for all flights on September 4, 6, 11, 12, 13, 14, 24, 25, and 26. Individual points are 1-min data and the linked red circles represent the median values in hourly bins of $P(O_3)$. Data are limited with the pressure altitude less than 1000 m to represent the lowest layer of the atmosphere.

The dependence of $P(O_3)$ on the NO mixing ratio ([NO]) shows that when the NO mixing ratio is less than ~1-2 ppbv, ozone production increases as the [NO] increases, i.e., $P(O_3)$ is in NOx sensitive regime for the all flights including the ones on September 25 and 26. When the NO mixing ratio is greater than ~1-2 ppbv, ozone production levels off as the NO mixing ratio further increases, i.e., $P(O_3)$ is in a NOx saturated regime (Figure 2-7). It was also found that at a given NO mixing ratio, a higher production rate of HOx results in a higher ozone

production rate, as points shown inside the circles in Figure 2-7. This is also true for the all flights including the ones on September 25 and 26.
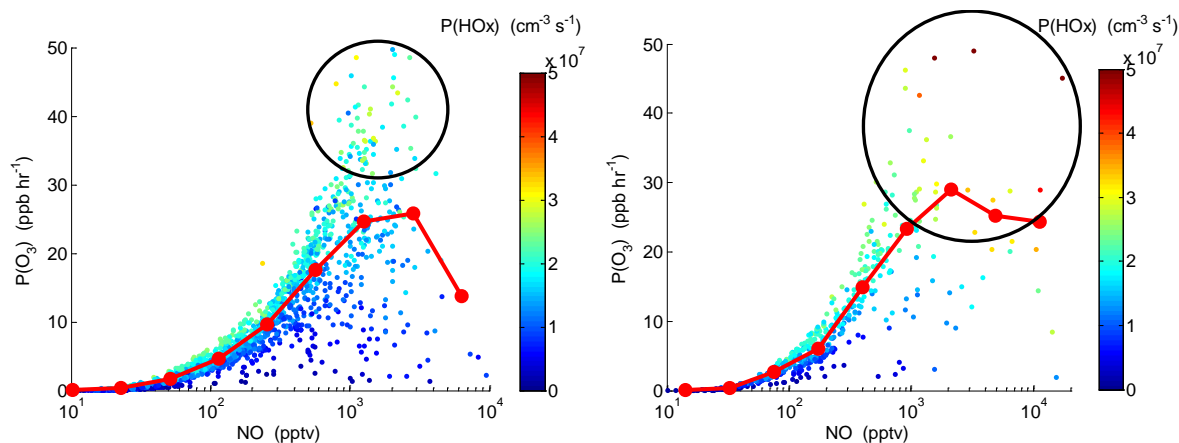
Figure 2-7. Ozone production as a function of NO mixing ratio. Individual data points are the 1 minute averages and are colored with the production rate of HOx (= OH + HO$_2$) during DISCOVER-AQ in Houston in 2013 for all flights except two flights on September 25 and 26 (***left***) and for two flights on September 25 and 26 (***Right***). The linked solid red circles represent the median values in [NO] bins. Note a log scale is used for the x axis.

Diurnal variations of the indicator of ozone production sensitivity to NOx and VOCs, L$_N$/Q, at eight individual locations where the P-3B conducted vertical spirals show that (1) at Deer Park, P(O$_3$) was mostly VOC sensitive for the entire day; (2) at Moody Tower and Channelview, P(O$_3$) was VOC sensitive or in the transition regime; and (3) at Smith Point and Conroe, P(O$_3$) is mostly NOx sensitive for the entire day (Figure 2-8).
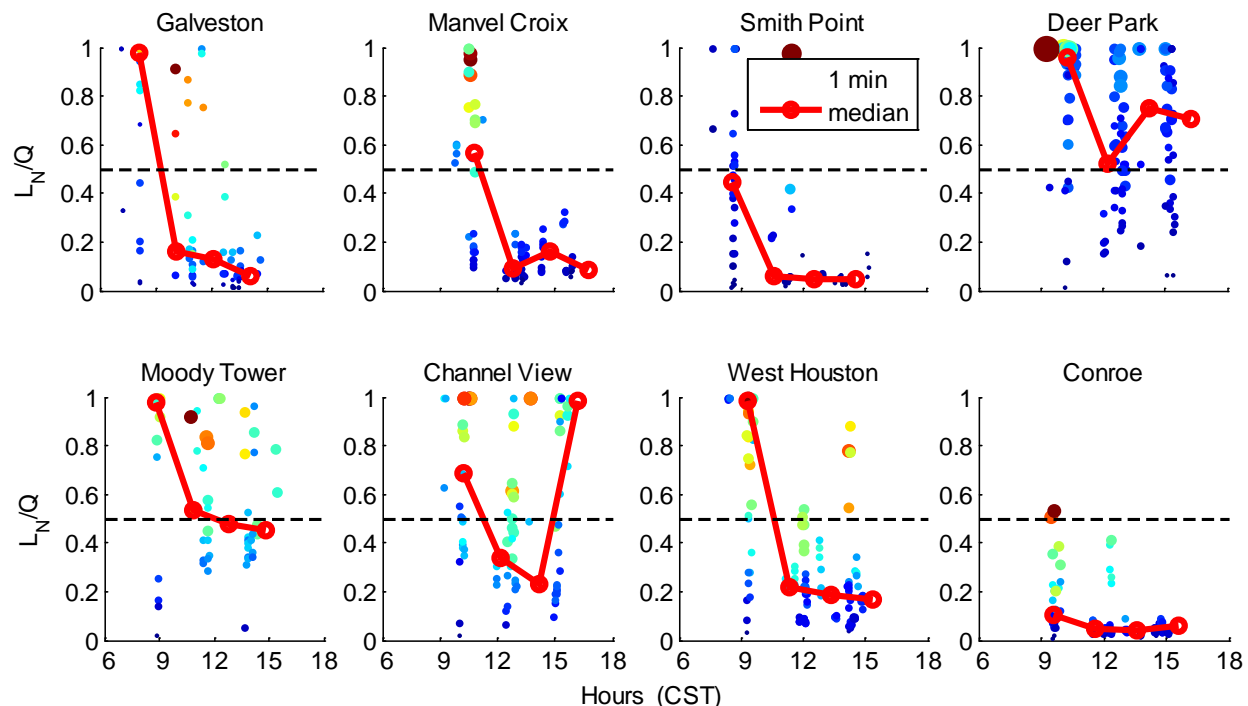
Figure 2-8. Diurnal variations of the indicator of ozone production sensitivity to NOx and VOCs, L_N/Q, at eight individual spiral locations during DISCOVER-AQ in Houston in 2013 for all flights on September 4, 6, 11, 12, 13, 14, 24, 25, and 26. Individual points are 1-min data and the linked red circles represent the median values in hourly bins of $P(O_3)$. Data are limited with the pressure altitude less than 1000 m to represent the lowest layer of the atmosphere.

2.4 OBJECTIVE 4. To calculate ozone production efficiency (OPE), defined as the ratio of the ozone production rate to the NOx oxidation rate, at different locations using the box and CMAQ model results.

Ozone production efficiency (OPE) is defined as the number of molecules of oxidant Ox ($=O_3+NO_2$) produced photochemically when a molecule of NOx ($=NO+NO_2$) is oxidized. It conveys information about the conditions under which O_3 is formed and is an important parameter to consider when evaluating impacts from NOx emission sources [Kleinman et al., 2002]. The OPE can be deduced from atmospheric observations as the slope of a graph of Ox concentration versus the concentration of NOx oxidation products. The latter quantity is denoted as NOz and is commonly measured as the difference between NOy (sum of all odd-nitrogen compounds) and NOx, i.e. NOz = NOy - NOx.

Figure 2-9 shows the photochemical oxidant Ox as a function of NOz ($=NOy-NOx$) during DISCOVER-AQ in Houston in 2013. Two data sets were plotted here. One is for the data collected on September 25 and 26, when high ambient ozone concentrations were observed. The other is for the data collected during all other flights. Note that the slopes obtained from these two data sets are essentially the same and an average OPE of ~8 is derived from the observations, meaning that 8 molecules of ozone were produced when one molecule of NOx was consumed. Even though higher ozone concentrations were observed on September 25 and 26, the OPE on these two days are not different from those in other flights, indicating the ozone event on

these two days was not caused by a higher OPE, but mainly, by higher concentrations of ozone precursors and background ozone as indicated by the intercepts in the regression of the two data sets in Figure 2-9.
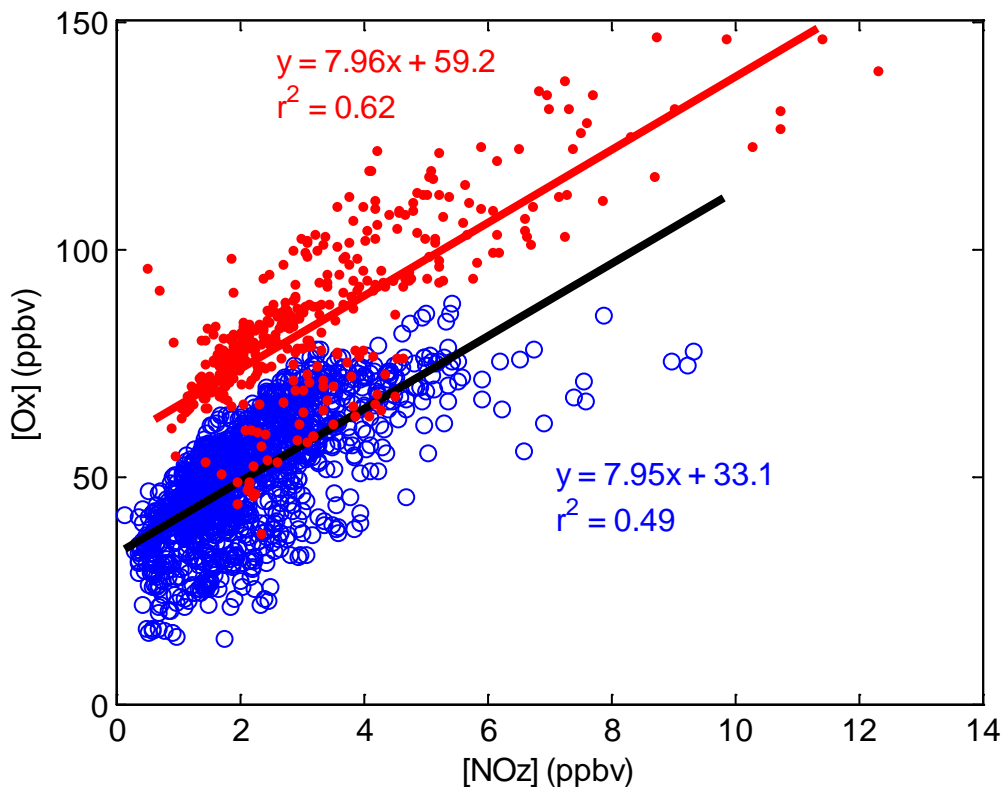
Figure 2-9. Photochemical oxidant, Ox (=O_3+NO_2) as a function of NOz (=NOy-NOx) during DISCOVER-AQ in Houston in 2013. Red dots are the data collected on September 25 and 26, 2013 when high ambient ozone concentrations were observed. Blue circles are the data collected during other flights. Data are limited with the pressure altitude less than 1000 m to represent the lowest layer of the atmosphere.

The OPE value during DISCOVER-AQ in Houston in 2013 is greater than the average OPE value (5.9±1.2) obtained during the Texas Air Quality Study in 2006 (TexAQS2006) [Neuman et al., 2009]. One possible reason for this increased OPE is the continuous reduction in NOx emissions in Houston between 2006 and 2013 pushed NOx levels closer to 1 ppbv in 2013, thus OPE increased since OPE increases as NOx decreases when the NOx level is greater than ~1 ppbv (Figure 2-11). This OPE value is about a factor of 1.5 to 2 higher than the OPEs obtained in the DISCOVER-AQ 2011 study in Maryland ranging from 4 to 5.5. This is mainly due to higher photochemical reactivity in Houston.

When calculating ozone production efficiency (OPE), it is important to know whether there is substantial loss of nitric acid (HNO_3), because it can affect the OPE by reducing the NOz [Trainer et al., 1993; 2000; Neuman et al., 2009]. The derived OPE in Figure 2-9 is only valid when there is minimum loss of NOz (especially HNO_3) from the source region to the point of observations. ΔCO/ΔNOy, i.e., the slope in a CO versus NOy plot, is an indicator for distinguishing plumes with efficient O_3 formation from plumes with similarly high O_3 to NOx

oxidation products correlation slopes caused by variable mixing of aged polluted air depleted in HNO_3 [Neuman et al., 2009].

The $\Delta CO/\Delta NOy$ was examined at different times of the day. For all flights but on September 25 and 26, the overall $\Delta CO/\Delta NOy$ was about 3.3 (Figure 2-10 (a)) throughout the day with a variation between 3.2 and 3.7 (Figure 2-10, (b)-(f)). For the two flights on September 25 and 26, the overall $\Delta CO/\Delta NOy$ was about 6.2 (Figure 2-10 (g)) throughout the day with a variation between 6.0 and 7.0 (Figure 2-10 (h)-(l)). This demonstrates that the observed O_3 formation was mainly from fresh plumes and was not caused by variable mixing of aged polluted air depleted in HNO_3.
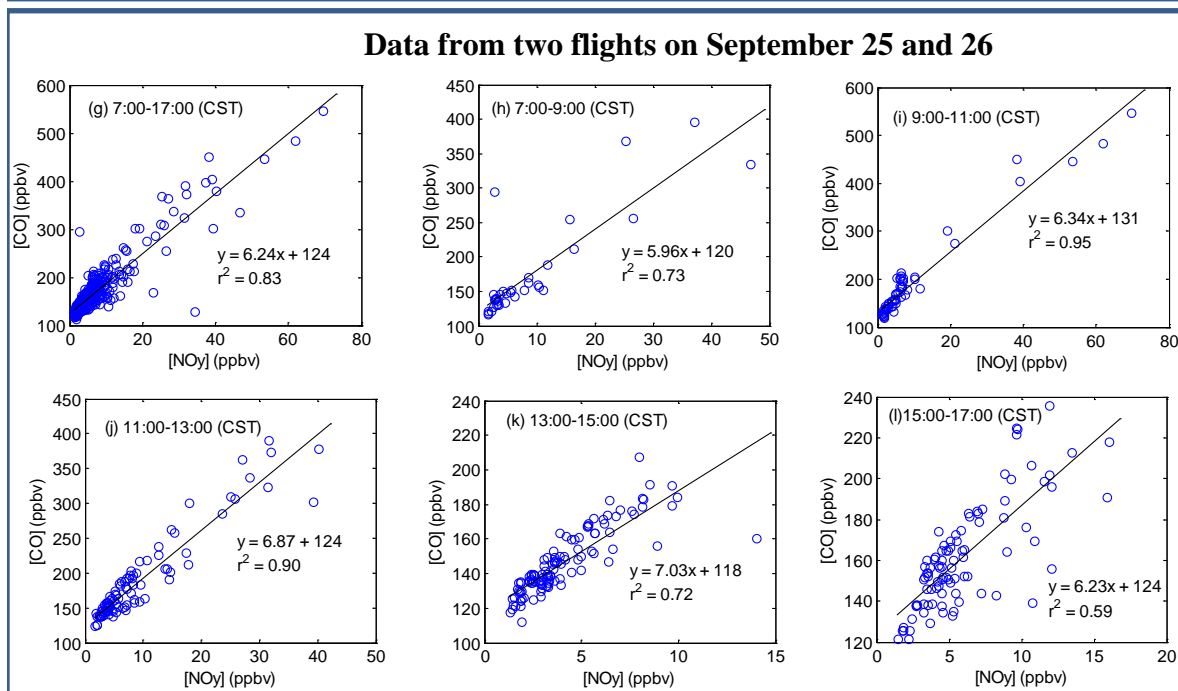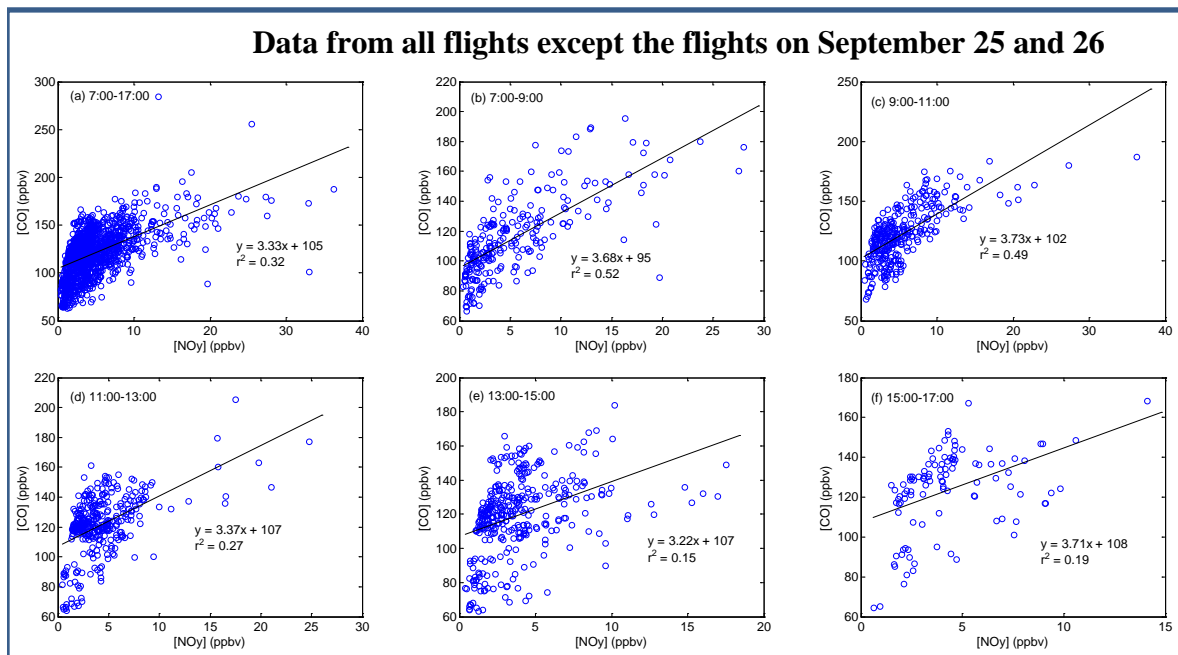
Figure 2-10. CO versus NOy and their linear regression during DISCOVER-AQ in Houston in 2013 for all flights except two flights on September 25 and 26 (***top (a)-(f)***) and for two flights on September 25 and 26 (***bottom (g)-(l)***) on September 25 and 26 at different times of the day: 07:00-17:00 (all data), 07:00-09:00, 09:00-11:00, 11:00-13:00, 13:00-15:00, and 15:00-17:00 (CST).

Using both the box model and CMAQ model (described in Appendix C and D) results, OPE can be also calculated according to its definition, i.e., the net ozone formation rate divided by of the formation rate of NOz. Net P(O$_3$) was calculated using Eq. (3), while the NOz formation rate is the sum of HNO$_3$ and organic nitrate formation rates. The agreement between the box model-derived and the CMAQ-derived OPEs is very good, with the mean OPEs of 15.8±7.4 (14.6±6.4 for two flight on September 25 and 26) in the box model and 17.0±11.1 (16.0±7.0 for two flight on September 25 and 26) in the CMAQ model. The dependence of OPE on NOx is also similar for both the box and CMAQ models (Figure 2-11). On average, the maximum of OPE appears at a NOx level around 1 ppbv. With the NOx level below 1 ppbv, OPE increases as the NOx level increases, while with the NOx level above 1 ppbv, OPE decreases as the NOx level increases (Figure 2-11). This is true for all flights including the two flights on September 25 and 26.
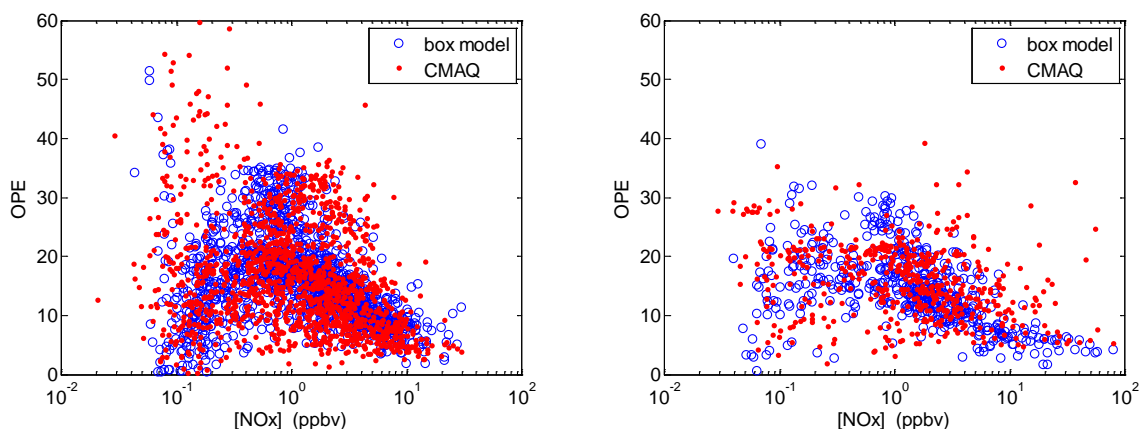
Figure 2-11. Ozone production efficiency (OPE) versus NOx in the box model (blue circles) and CMAQ model (red dots) results during DISCOVER-AQ in Houston in 2013 for all flights except two flights on September 25 and 26 (***left***) and for two flights on September 25 and 26 (***Right***). OPE is calculated according to its definition as the net ozone formation rate divided by of the formation rate of NOz.

It is worth noting that the OPE values calculated using the CMAQ and box model results are greater than the values derived from the observations using the slope in the scatter plot of Ox versus NOz in Figure 2-9. This is expected because in the calculation of OPE using the box and CMAQ model results, a few ozone loss processes, such as ozone dry deposition and horizontal/vertical dispersion, even though they are important, were not considered in the calculation, which results in higher calculated ozone production rates using the model results. This is certainly the limitation of the models regarding this calculation.

Spatial variations of OPE demonstrate that except a few hotspots over Downtown Houston and Houston Ship Channel, most large OPEs appear away from the urban center, e.g.,

the northwest and southeast of the area, while in areas with high NOx emissions close to the urban center lower OPEs were generally observed (Figure 2-12). This is true for all flights including the two flights on September 25 and 26. This is again consistent with the results in Figure 2-11 that the maximum of OPE appears at a NOx level around 1 ppbv. Even though the highest ozone concentration was observed on September 25 during DISCOVER-AQ, the OPE on these two days was not the highest, mainly because of higher NOx levels (higher than 1 ppbv) on these two days than on other flight days.
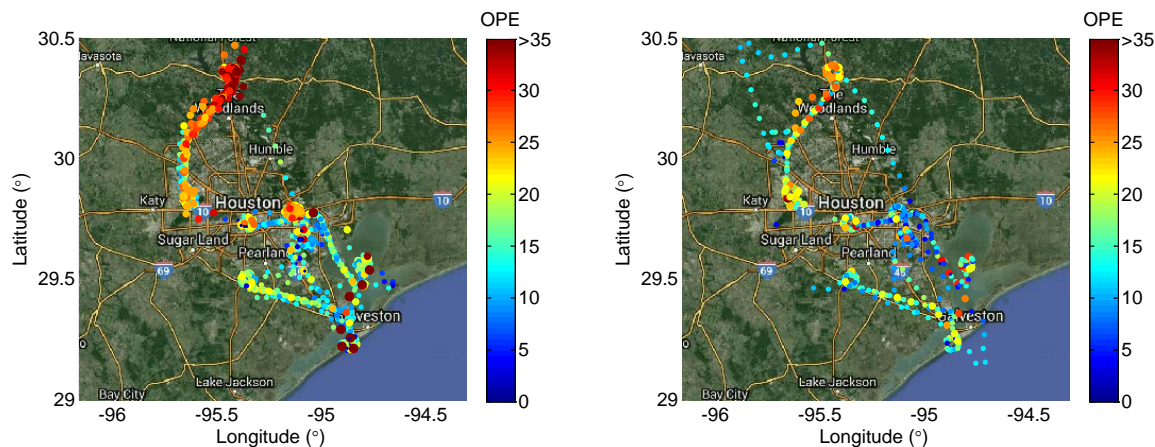
Figure 2-12. Ozone production efficiency (OPE) along the P-3B flight track during DISCOVER-AQ in Houston in 2013 for all flights except two flights on September 25 and 26 (*left*) and for two flights on September 25 and 26 (***Right***). OPE was calculated using the box model results as the ratio of net ozone formation rate to the formation rate of NOz.

3. PROJECT SUMMARY

The following is a summary of the primary conclusions from our data analysis of the DISCOVER-AQ campaign in Houston in 2013:

(1) On average ozone production, $P(O_3)$, was about 20-30 ppbv hr^{-1} in the morning and 5-10 ppbv hr^{-1} in the afternoon during DISCOVER-AQ in Houston in 2013. The diurnal variation of $P(O_3)$ shows a broad peak in the morning with significant $P(O_3)$ in the afternoon obtained on ten flight days in September 2013. It is noticed that high $P(O_3)$ mainly occurred with L_N/Q is greater than 0.5, i.e., in the VOC sensitive regime.

(2) Ozone production rate depends on NOx level and radical production rate. $P(O_3)$ increases as [NO] increases up to ~1 ppbv and then levels off with further increase of [NO]. At a given [NO], a higher production rate of HOx results in a higher ozone production rate. This has some implications for the NOx control strategies in order to achieve the ozone control goal.

(3) Hotspots of $P(O_3)$ over Downtown Houston and Houston Ship Channel were observed due to significant emission sources in this area.

(4) Diurnal variations of ozone production rate at eight individual locations where the P-3B conducted vertical spirals show that the ozone production rate is on average more than 10 ppbv hr^{-1} at locations with high NOx and VOC emissions such as Deer Park, Moody Tower and Channelview, while at locations away from the urban center with lower emissions of ozone precursors such as Galveston, Smith Point, and Conroe, the ozone production rate is usually less than 10 ppbv hr^{-1} on average.

(5) Ozone production tended to be more VOC sensitive in the morning with high $P(O_3)$. The diurnal variation of L_N/Q indicates that $P(O_3)$ was mainly VOC sensitive in the early morning and then transited towards the NOx sensitive regime later in the day. High $P(O_3)$ in the morning was mainly associated with VOC sensitivity due to high NOx levels in the morning. This suggests that control of VOC may be an effective way to control O_3.

(6) Ozone production was generally NOx sensitive in the afternoon with spatial variations, even though there were periods when $P(O_3)$ was VOC sensitive. At Deer Park, $P(O_3)$ was mostly VOC sensitive for the entire day. At Moody Tower and Channelview, $P(O_3)$ was VOC sensitive or in the transition regime. At Smith Point and Conroe, $P(O_3)$ was mostly NOx sensitive for the entire day.

(7) Ozone production efficiency (OPE) was about 8 during DISCOVER-AQ 2013 in Houston, i.e., 8 molecules of ozone were produced when one molecule of NOx was consumed. This OPE value is greater than the average OPE value (5.9±1.2) obtained during the Texas Air Quality Study in 2006 (TexAQS2006) [Neuman et al., 2009]. One possible reason for this increased OPE is the continuous reduction in NOx emissions in Houston between 2006 and 2013 pushed NOx levels closer to 1 ppbv in 2013, thus OPE increased since OPE increases as NOx decreases when the NOx level is greater than ~1 ppbv (Figure 2-11). This OPE value is about a factor of 1.5 to 2 higher than the OPE obtained in the DISCOVER-AQ 2011 study in Maryland due to higher photochemical reactivity in Houston.

4. REFERENCES

Atkinson, R., et al., Evaluated kinetic and photochemical data for atmospheric chemistry: Volume I - gas phase reactions of Ox, HOx, NOx and SOx species, *Atmos. Chem. Phys.*, 4, 1461-1738, 2004.

Atkinson, R., et al., Evaluated kinetic and photochemical data for atmospheric chemistry: Volume II - gas phase reactions of organic species, *Atmos. Chem. Phys.*, 6, 3625-4055, 2006

Atkinson, R., et al., Evaluated kinetic and photochemical data for atmospheric chemistry: Volume III - gas phase reactions of inorganic halogens, *Atmos. Chem. Phys.*, 7, 981-1191, 2007.

Atkinson, R., et al., Evaluated kinetic and photochemical data for atmospheric chemistry: Volume IV - gas phase reactions of organic halogen species, *Atmos. Chem. Phys.*, 8, 4141-4496, 2008.

Banta, R., C. J. Senff, J. Nielsen-Gammon, L. Darby, T. Ryerson, R. Alvarez, P. Sandberg, E. Williams, and M. Trainer, A bad air day in Houston, *Bullet. Am. Meteorol. Soc.*, 86, 657-669, doi: 10.1175/BAMS-86-5-657, 2005.

Carpenter, L.J., S.M. MacDonald, M.D. Shaw, R. Kumar, R.W. Saunders, R. Parthipan, J. Wilson, J.M.C. Plane, 2013. Atmospheric iodine levels influenced by sea surface emissions of inorganic iodine. *Nature Geoscience Letters*, 6, 108-111.

Chen, S., X. Ren, J. Mao, Z. Chen, W. H. Brune, , B. Lefer, B. Rappenglück, J. Flynn, J. Olson, J. H. Crawford, A comparison of chemical mechanisms based on TRAMP–2006 field data, *Atmos. Environ.*, 44(33), 4116-4125, 2010.

Chen, F., S. Miao, M. Tewari, J.-W. Bao, and H. Kusaka, A numerical study of interactions between surface forcing and sea breeze circulations and their effects on stagnation in the greater Houston area, J. Geophys. Res., 116, D12105, doi:10.1029/2010JD015533, 2011.

Darby, L. S., Cluster analysis of surface winds in Houston, Texas, and the impact of wind patterns on ozone, *J. Appl. Meteorol.*, 44, 1788-1806, doi:10.1175/JAM2320.1, 2005.

DISCOVER-AQ whitepaper, http://discover-aq.larc.nasa.gov/pdf/DISCOVER-AQ_science.pdf.

Emmons, L.K., S. Walters, P.G. Hess, J-F Lamarque, G.G. Pfister, D. Fillmore, C. Granier, A. Guenther, D. Kinnison, and T. Laepple. "Description and Evaluation of the Model for Ozone and Related Chemical Tracers, Version 4 (mozart-4), Geoscientific Model Development, 3, 43–67, 2010.

Flynn, C. M., K. E. Pickering, J. H. Crawford, L. Lamsal, N. Krotkov, J. Herman, A. Weinheimer, G. Chen, X. Liu, J. Szykman, S.-C. Tsay, C. P. Loughner, J. Hains, P. Lee, R. R. Dickerson, J. W. Stehr, L. Brent, The Relationship between Column-density and Surface Mixing Ratio: Statistical Analysis of O_3 and NO_2 Data from the July 2011 Maryland DISCOVER-AQ Mission, Submitted to Atmos. Environ, 2013.

Finlayson-Pitts, B. J., and J. Pitts, Chemistry of the upper and lower atmosphere: Theory, experiments and applications, p.264-276, Academic Press, San Diego, California, 2000.

Goliff, W. S., W. R. Stockwell, and C. V. Lawson, The Regional Atmospheric Chemistry Mechanism, Version 2, Atmos. Environ., 68, 174–185, doi:10.1016/j.atmosenv.2012.11.038, 2013

Goldberg, D. L., C. P. Loughner, M. Tzortziou, J. W. Stehr, K.E. Pickering, L. T. Marufu, J. H. Crawford, A. Mannino, and R. R. Dickerson, Surface ozone concentrations over the Chesapeake Bay during DISCOVER-AQ, Atmos. Environ., in press, 2013.

He, H., C. P. Loughner, J. W. Stehr, H. L. Arkinson, L. C. Brent, M. B. Follette-Cook, M. A. Tzortziou, K. E. Pickering, A. M. Thompson, D. K. Martins, G. S. Diskin, B. E. Anderson, J. H. Crawford, A. J. Weinheimer, P. Lee, J. C. Hains, and R. R. Dickerson, An elevated

reservoir of air pollutants over the Mid-Atlantic States during the 2011 DISCOVER-AQ campaign: Airborne measurements and numerical simulations, Atmos. Environ., in press, 2013.

Houyoux, M. R. and J. M. Vukovich, Updates to the Sparse Matrix Operator Kernel Emissions (SMOKE) Modeling System and Integration with Models-3, presented at The Emission Inventory: Regional Strategies for the Future, Air and Waste Management Association, Raleigh, NC, 1999.

Jacob, D. J., Introduction to Atmospheric Chemistry, Princeton University Press, New Jersey, 1999.

Kleinman, L. I., P. H. Daum, Y.-N Lee, L. J. Nunnermacker, S. R. Springston, J. Weinstein-Lloyd, and J. Rudolph, Sensitivity of ozone production rate to ozone precursors. Geophys. Res. Lett., 28, 2903–2906 , doi: 10.1029/2000GL012597, 2001.

Kleinman, L. I., P. H. Daum, Y.-N. Lee, L. J. Nunnermacker, S. R. Springston, J. Weinstein-Lloyd, and J. Rudolph, Ozone production efficiency in an urban area, J. Geophys. Res., 107 (D23), 4733, doi:10.1029/2002JD002529, 2002

Kleinman, L. I., P. H. Daum, Y.-N. Lee, L. J. Nunnermacker, S. R. Springston, J. Weinstein-Lloyd, and J. Rudolph, A comparative study of ozone production in five U.S. metropolitan areas, J. Geophys. Res., 110, D02301, doi:10.1029/2004JD005096, 2005a.

Kleinman, L. I., The dependence of tropospheric ozone production rate on ozone precursors, Atmos. Environ., 39(3), 575–586, doi:10.1016/j.atmosenv.2004.08.047, 2005b.

Lei, W., R. Zhang, X. Tie, and P. Hess, Chemical characterization of ozone formation in the Houston-Galveston area: A chemical transport model study, J. Geophys. Res., 109, D12301, doi:10.1029/2003JD004219, 2004.

Li, G., R. Zhang, J. Fan, and X. Tie, Impacts of biogenic emissions on photochemical ozone production in Houston, Texas, J. Geophys. Res., 112, D10309, doi:10.1029/2006JD007924, 2007.

Loughner, C. P., D. J. Allen, K. E. Pickering, R. R. Dickerson, D. -L. Zhang , Roles of urban tree canopy and buildings in urban heat island effects: parameterization and preliminary results, Journal of Applied Meteorology and Climatology, 51, 1775-1793, 2012.

Loughner, C. P., D. J. Allen, K. E. Pickering, R. R. Dickerson, D. -L. Zhang, Y. -X. Shou, Impact of fair-weather cumulus clouds and the Chesapeake Bay breeze on pollutant transport and transformation, Atmos. Environ., 45, 4060-4072, 2011.

Loughner, C.P., B. Duncan, M. Follette-Cook, J. Hains, K.E. Pickering, M. Tzortziou, Y. Yoshida, Impact of historical air pollution emissions reductions on surface ozone during record breaking heat, presented at 12th Annual CMAS Conference, Chapel Hill, NC., 2013.

Loughner, C. P., M. Tzortziou, M. Follette-Cook, K.E. Pickering, D. Goldberg, C. Satam, A. Weinheimer, J.H. Crawford, D.K. Knapp, D.D. Montzka, G.B. Diskin, L.T. Marufu, and R.R. Dickerson, Impact of bay breeze circulations on surface air quality and boundary layer export, submitted to Journal of Applied Meteorology and Climatology, 2013a.

Mallet, V. and B. Sportisse, B., A comprehensive study of ozone sensitivity with respect to emissions over Europe with a chemistry-transport model, J. Geophys. Res., 110, D22302, doi:10.1029/2005JD006234, 2005.

Mao, J., X. Ren, S. Chen, W. H. Brune, Z. Chen, M. Martinez, H., Harder, B. Lefer, B. Rappenglück, J. Flynn, and M. Leuchner, Atmospheric oxidation capacity in the summer of Houston 2006: Comparison with summer measurements in other metropolitan studies, *Atmos. Environ.*, 44(33), 4107-4115, 2010

Molina, M. J., and L. T. Molina, Megacities and atmospheric pollution, J. Air Waste Manage., 54, 644–680, 2004.

Morris, R. E., Yarwood, G., Emery, C. A., and B. Koo, Development and Application of the CAMx Regional One-atmospheric Model to Treat Ozone, Particulate Matter, Visibility, Air Toxics and Mercury." Air & Waste Management Association's 97th Annual Conference and Exhibition, 2004

Neuman, J. A., et al. (2009), Relationship between photochemical ozone production and NOx oxidation in Houston, Texas, *J. Geophys. Res.*, 114, D00F08, doi:10.1029/2008JD011688.

Parrish, D.D., D.T. Allen, T.S. Bates, M. Estes, F.C. Fehsenfeld, G. Feingold, R. Ferrare, R.M. Hardesty, J.F. Meagher, J.W. Nielsen-Gammon, R.B. Pierce, T.B. Ryerson, J.H. Seinfeld, and E.J. Williams, 2009. Overview of the Second Texas Air Quality Study (TexAQS II) and the Gulf of Mexico Atmospheric Composition and Climate Study (GoMACCS), Journal of Geophysical Research, 114, D00F13, doi:10.1029/2009JD001842, 2009.

Ren, X., D. van Duin, M. Cazorla, S. Chen, J. Mao, L. Zhang, W. H. Brune, J. H. Flynn, N. Grossberg, B. L. Lefer, B. Rappenglück, K. W. Wong, C. Tsai, J. Stutz, J. E. Dibb, B. T. Jobson, W. T. Luke, and P. Kelley, Atmospheric oxidation chemistry and ozone production: Results from SHARP 2009 in Houston, Texas, J. Geophys. Res., 118, 5770–5780, 2013.

Sander, S. P., J. Abbatt, J. R. Barker, J. B. Burkholder, R. R. Friedl, D. M. Golden, R. E. Huie, C. E. Kolb, M. J. Kurylo, G. K. Moortgat, V. L. Orkin and P. H. Wine, Chemical Kinetics and Photochemical Data for Use in Atmospheric Studies, Evaluation No. 17, JPL Publication 10-6, Jet Propulsion Laboratory, Pasadena, 2011 (http://jpldataeval.jpl.nasa.gov).

Sillman, S., The use of NO_y, H_2O_2, and HNO_3 as indicators for O_3-NO_x-hydrocarbon sensitivity in urban locations, J. Geophys. Res., 100, 14,175–14,188, 1995.

Sillman, S., R. Vautard, L. Menut, and D. Kley, O_3-NO_x-VOC sensitivity and NO_x-VOC indicators in Paris: Results from models and Atmospheric Pollution Over the Paris Area (ESQUIF) measurements, J. Geophys. Res., 108(D17), 8563, doi:10.1029/2002JD001561, 2003.

Skamarock, W.C., J.B. Klemp, J. Dudhia, D.O. Gill, D.M. Barker, W. Wang, and J.G. Powers, A Description of the Advanced Wrf Version 3." NCAR technical note NCAR/TN/u2013475+ STR, 2008

Stauffer, R. M., A. M. Thompson, D. K. Martins, R. D. Clark, D. L. Goldberg, C. P. Loughner, R. Delgado, R. R. Dickerson, J. W. Stehr, and M. A. Tzortziou , Bay breeze influence on surface ozone at Edgewood, MD during July 2011, J. Atmos. Chem., doi: 10.1007/s10874-012-9241-6, 2013.

Tang, X., Wang, Z., Zhu, J., Gbaguidi, A. E., Wu, Q., Li, J., and Zhu, T., Sensitivity of ozone to precursor emissions in urban Beijing with a Monte Carlo scheme. Atmos. Environ., 44, 3833-3842, 2010.

Texas Air Quality Research Program, TCEQ Priority Research Areas, 2013 (available at http://aqrp.ceer.utexas.edu/docs/FY14-15/FINAL_AQRP%20Priorities%20Research%20Areas%202014-15%20(2).pdf)

Trainer, M., et al. (1993), Correlation of ozone with NOy in photochemically aged air, J. Geophys. Res., 98, 2917 – 2925, doi:10.1029/ 92JD01910.

Trainer, M., D. D. Parrish, P. D. Goldan, J. Roberts, and F. C. Fehsenfeld (2000), Review of observation-based analysis of the regional factors influencing ozone concentrations, Atmos. Environ., 34, 2045 – 2061, doi:10.1016/S1352-2310(99)00459-8.

Tzortziou, M., J. R. Herman, A. Cede, C. P. Loughner, N. Abuhassan, and S. Naik, Spatial and temporal variability of ozone and nitrogen dioxide over a major urban estuarine ecosystem, Journal of Atmospheric Chemistry, doi:10.1007/s10874-013-9255-8, 2013.

Vukovich, J. and T. Pierce. The Implementation of BEIS-3 within the SMOKE modeling framework, presented at Emissions Inventories – Partnering for the Future, paper presented at

the 11th Emissions Inventory Conference of the U.S. Environmental Protection Agency, Research Triangle Park, NC, 2002.

Wiedinmyer, C., S. K. Akagi, R. J. Yokelson, L. K. Emmons, J. A. Al-Saadi, J. J. Orlando, and A. J. Soja, The Fire INventory from NCAR (FINN): A high resolution global model to estimate the emissions from open burning, Geosci. Model Develop., 4, 625-641, doi:10.5194/gmd-4-625-2011, 2011.

Xue, L. K., T. Wang, J. Gao, A. J. Ding, X. H. Zhou, D. R. Blake, X. F. Wang, S. M. Saunders, S. J. Fan, H. C. Zuo, Q. Z. Zhang, and W. X. Wang, Ozone production in four major cities of China: sensitivity to ozone precursors and heterogeneous processes, Atmos. Chem. Phys. Discuss., 13, 27,243–27,285, doi:10.5194/acpd-13-27243-2013, 2013.

Yarwood, G., S. Rao, M. Yocke, M., and G. Z. Whitten, Updates to the Carbon Bond Mechanism: CB05, Final Report to the US EPA (RT-0400675), 2005 (http://www.camx.com/publ/ pdfs/CB05_Final_Report_120805.pdf).

5. AUDITS OF DATA QUALITY

5.1 QUALITY ASSURANCE CHECKS

This section identifies the Quality Assurance (QA) checks (e.g., blanks, control samples, duplicates, matrix spikes, surrogates), the frequencies for performing these checks, associated acceptance criteria, and corrective actions to be performed if acceptance criteria are not met for each process measurement and analytical method.

The general QA/QC checks for the O_3, NO, NO_2, NO_Y, total peroxyl nitrates, total alkyl nitrates, HCHO, CO_2, CO, CH_4, H_2O, and VOCs measurements on the P-3B are described in the table below, along with acceptance criteria.

Table 5-1. QA/QC checks for the trace gas measurements on the NASA P-3B during the DISCOVER-AQ 2013 in Houston.

Assessment Parameter	Quality Control Procedure	Minimum Frequency	Acceptance Criteria	Corrective Action
Measurement system contribution - Calibration	Precision/Linearity test – Multipoint calibration	Once per flight, and prior to and following installation, repair, or adjustment of equipment	Linear fit of 0.995 or better	Check calibrator settings. Recalibrate or repair.
Measurement system contribution – Span Check	Span checks	Each flight, and prior to and following installation, repair, or adjustment of equipment	Relative Standard Deviation < 5%	Check calibrator settings. Recalibrate or repair.
Measurement system contribution – Zero Check	Zero offset check	Several times per flights	Response below detection limit	Check zero air supply. Check for leaks. Adjust zero offset.

5.2 ACCEPTANCE CRITERIA

This section addresses any additional project-specific QA objectives (e.g., completeness, mass balance) shall be presented, including acceptance criteria.

See Table 5-1 in Section 5.1 above for acceptance criteria.

5.3 DATA QUALITY AUDITS

More than 10% of the CB05 box model and WRF-CMAQ model input and output files, scripts, and analysis products were reviewed for quality assurance purposes. Model inputs and outputs, model evaluation statistics, and graphics generated for this project are being stored and will continue to be for at least three years after the completion of the project at the University of Maryland. In addition, all model inputs, outputs, and post-processing analyses will be sent to the University of Texas after the completion of the project.

6. RECOMMENDATIONS FOR FUTURE WORK

Based on the results from this work, the following recommendations are made for future work:

(1) In future field studies, when it is feasible, a complete suite of VOC measurements are desired in order to accomplish more rigid and accurate box model simulations. Missing those measurements could potentially cause a large uncertainty in the model results.

(2) Because of the spatial and temporary variations of ozone production and its sensitivity, comprehensive observations of air pollutants at different representative locations in the studied area are needed in order to form a non-uniform emission reduction strategy.

(3) Calculation of ozone production efficiency (OPE) using observed ΔOx and ΔNOz needs to be done only when there is no significant loss of HNO_3 from source regions to the point where observations are made. As suggested by Neuman et al. [2009], the ratio of $\Delta CO/\Delta NOy$ provides an indicator for distinguishing plumes with efficient O_3 formation from plumes with similarly high OPE slopes caused by variable mixing of aged polluted air depleted in HNO_3, thus it should be used to examine if there is a significant loss of HNO_3 before using $\Delta Ox/\Delta NOz$ to calculate OPE.

(4) In future field campaigns, results from 3-dimensional chemical transport models should be compared to the results from box model that is constrained with field observations to examine atmospheric photochemistry and to reveal potential uncertainties associated with the chemical transport models.

(5) In future air quality studies in Houston and Texas, the relative contributions to ozone production from biogenic and anthropogenic emissions of VOCs need to be investigated in order to reach a realistic VOC emission control strategy since the biogenic VOC emissions cannot be controlled.

7. ACKNOWLEDGEMENT/DISCLAIMER

8. APPENDIX A - MEASUREMENT PROCEDURES (DISCOVER-AQ DATA COLLECTION)

The measurements during the DISCOVER-AQ 2013 in Houston were mainly made from the NASA P-3B aircraft and eight surface monitoring stations, including Smith Point, Galveston, Manvel Croix, Deer Park, Channelview, Conroe, West Houston, and Moody Tower. The major airborne platform selected for the DISCOVER-AQ mission was the P-3B. The P-3B is an ideal choice for a profiling aircraft for several reasons: 1) it is capable of hosting a comprehensive atmospheric chemistry and aerosol payload, 2) it is ideal for profiling the lower atmosphere, and 3) it has sufficient flight duration (eight hours) for sampling throughout the day [DISCOVER-AQ whitepaper].

The eight surface sites chosen for the deployment were evaluated prior to DISCOVER-AQ with regard to the presence or absence of complementary chemical and meteorological measurements which enhanced the utility of aircraft measurement suite; the nature, strength, and likely impact of nearby point and mobile emission sources; the nature, height, and extent of nearby structures and vegetation, and their likely influence on local meteorology and wind flow patterns; and any other characteristic which might render the site physically or chemically unrepresentative of the surrounding area [DISCOVER-AQ whitepaper].

8.1 ANALYTICAL METHODS

This section describes or references each process measurement or analytical method used. If applicable, modifications to EPA-approved or similarly validated methods are identified.

Table 5-1 lists specifications for the P-3B in situ trace gas measurements. All of these investigators fielded their instruments onboard the NASA DC-8 during the recent ARCTAS field campaign in 2008 [Jacob et al., 2009], and all have experience on other airborne platforms (e.g., NASA P-3B, NSF C-130, and NSF HIAPER).

Table 8-1. P-3B in situ trace gas measurements1

Co-I	Technique or Instrument	Species	Precision	Uncertainty
Cohen	Thermal-Dissociation, Laser-Induced Fluorescence	NO_2	10 pptv	5%
		Total Peroxy Nitrates	40 pptv	10%
		Total Alkyl Nitrates	50 pptv	15%
		HNO_3	50 pptv	20%
Weinheimer	Chemiluminescence	O_3	0.1 ppbv	5%
		NO and NO_y	20 pptv	10%
		NO_2	20 pptv	10-20%
Fried	IR Absorption Spectrometer	CH_2O	60-80 pptv	12%
Vay	modified LI-COR 6252	CO_2	0.1 ppmv	0.25 ppm
Diskin	Diode Laser Spectrometer	CO	1 ppbv	1.5%
		CH_4	2 ppbv	0.2%
	Diode Laser Hygrometer	H_2O	0.1%	5%
Wisthaler	Proton Transfer Reaction-Mass Spectrometer	methanol	100 pptv	20%
		acetaldehyde	100 pptv	15%
		acetone	50 pptv	10%
		isoprene, MVK/MACR	20 pptv	10%
		acetonitrile	10 pptv	10%
		benzene, toluene, C8-aromatics, C9-aromatics	10 pptv	10%

1-response time for all instruments is 1 s with exception of Wisthaler which has 10 s response.

Table 5-2 lists specifications for the P-3B in situ aerosol measurements fielded by Dr. Bruce Anderson. With the exception of the last three instruments in the table, Dr. Anderson has fielded this measurement suite many times, most recently during ARCTAS. The final three instruments were fielded during ARCTAS by other investigators, thus their airborne implementation and integration is well demonstrated.

Table 8-2. P-3B in situ aerosol measurements

Technique/Instrument	Response	Parameter	Precision	Size Range
Condensation Particle Counters (TSI 3025, TSI 3010)	1 s	Ultrafine, Nonvolatile CN	10%	>0.003
TSI Scanning Mobility Particle Sizer	60 s	Aerosol Particle Size	20%	0.01 – 0.3
DMT Ultra-High Sensitivity Aerosol Spectrometer	1 s		20%	0.08 – 1.0
MetOne Optical Particle Counter	1 s		40%	0.3 – 10
Aerodynamic Particle Sizer (TSI 3321)	1 s		20%	0.5 – 20
DMT Cloud Condensation Nuclei counter	1 s	Cloud Condensation Nuclei Spectra	NA	<10
Nephelometer (TSI 3563)	1 s	Scattering at 450, 550, and 700 nm	5e-7 mM or 5%	<10
Particle Soot Absorption Photometer	5-60 s	Absorption at 467, 530, and 660 nm	5e-7 mM or 5%	<10
RR Nephelometers	20 s	Humidity Dependence of Scattering	NA	<10
DMT Single Particle Soot Photometer	1 s	Black Carbon	20%	0.1 – 1.0
Particle into Liquid Sampler/Ion Chromatograph	300 s	Soluble Ion Composition	NA	0.01 – 1.0
Particle into Liquid Sampler/Total Organic Carbon	30 s	Water Soluble Organic Carbon	NA	0.01 – 1.0

Table 5-3 lists specifications for the P-3B navigational and meteorological observations. While these observations are often considered to be turn-key, experience has shown that loss of data or lack of adequate QC for these data can be detrimental to mission success. Mr. John Barrick has more than a decade of experience in providing these observations on the P-3B and was responsible for collecting and reporting these data during DISCOVER-AQ.

Table 8-3. P-3B navigational and meteorological measurements

Parameter	Response	Technique/Instrument	Precision
GPS Location	1 s	GPS/Trimble TNL-3000	15 m
GPS Altitude	1 s		50 m
Pressure	1 s	MEMS/Rosemount MADT 2014	0.3 mb
Pressure Altitude	1 s	Calculated/Rosemount MADT 2014	5 m
Radar Altitude	1 s	Radar Altimeter/ Honeywell AA-300	3 m
Pitch, Roll, and Heading	1 s	INS/Honeywell Laseref	0.2 °
Wind Speed and Direction	1 s		3 m/s; ± 10 °
Ground Speed and Track	1 s		1 m/s; 0.5 °
True Air Speed	1s		2 m/s
Temperature	1 s	PRT/Rosemount E102 Non-Deiced	0.2 °C
Dew/Frost point	2 - 30 s	Edgetech Vigilant 137 3-Stage Chilled Mirror Hygrometer	0.5 - 1.0 °C
NO_2 Photolysis Frequency	1 s	Metcon jNO_2 Filter Radiometers	8%

9. APPENDIX C – DATA ANANLYSIS METHODS

A chemical transport model (WRF-CMAQ) and a box model (based on CB05) were used to analyze the data collected during DISCOVER-AQ 2013 in Houston.

(1) WRF-CMAQ Model Simulations

This project utilized the WRF and CMAQ models run down to a horizontal resolution of 4 km that covers the entire DISCOVER-AQ field campaign. WRF and CMAQ model descriptions can be found on their respective webpages: www.wrf-model.org and www.cmaq-model.org. The WRF model was driven by the 12 km North American Mesoscale (NAM) model and the Multi-scale Ultra-high Resolution (MUR) sea surface temperature analysis (http://podaac.jpl.nasa.gov/Multi-scale_Ultra-high_Resolution_MUR-SST). The CMAQ model utilized chemical initial and boundary conditions from the Model for Ozone And Related Chemical Tracers (MOZART) Chemical Transport Model (CTM) (https://www2.acd.ucar.edu/gcm/mozart) and the CB05 chemical mechanism. The 2012 baseline anthropogenic emissions from the Texas Commission on Environmental Quality (TCEQ) were used as input to CMAQ. These emissions contain the most-up-to-date Texas anthropogenic emissions inventory and a compilation of emissions estimates from Regional Planning Offices throughout the US Biogenic emissions was calculated online within CMAQ with Biogenic Emission Inventory System (BEIS). Biomass burning emissions came from the Fire Inventory from National Center for Atmospheric Research (NCAR) Version 1 (FINNv1), and lightning emissions were calculated online within CMAQ.

Two sets of WRF and CMAQ model simulations were performed covering the DISCOVER-AQ Texas field deployment for Texas AQRP Project # 14-004, an original and an improved set. CMAQ was re-run based on the improved WRF and CMAQ simulations for this project with the process analysis tool to determine NOx and VOC sensitive regimes and ozone production and loss rates. All CMAQ inputs used in running the improved CMAQ run for Texas AQRP Project # 14-004 were utilized in this project. The method of running the improved WRF and CMAQ simulations, which is reported in the Final Report for Texas AQRP Project #14-004 is reviewed here.

WRF and CMAQ were initialized on August 18, 2013 to allow for adequate model spin-up time. WRF was run with nested domains with horizontal resolutions of 36, 12, 4, and 1 km and are shown in Figures 1 and 2. This project only utilized the 4 km domain. The WRF and CMAQ simulations employ 45 vertical levels extending from the surface to 50 mb (Table 1). The WRF simulation utilized the Multi-scale Ultra-high Resolution (MUR) Sea Surface Temperature (SST) Analysis, which has a horizontal resolution of about 1 km (available at: http://podaac.jpl.nasa.gov/Multi-scale_Ultra-high_Resolution_MUR-SST). The 12 km North American Mesoscale (NAM) model was used for meteorological initial and boundary conditions and analysis nudging. WRF and CMAQ configuration options are shown in Table 2. The WRF simulation employed observational nudging of the National Centers for Environmental Prediction (NCEP) Automated Data Processing (ADP) Global Surface (http://rda.ucar.edu/datasets/ds461.0/) and Upper Air (http://rda.ucar.edu/datasets/ds351.0/) Observational Weather Data. Observational and analysis nudging were performed on all domains. Model output was saved hourly for the 36 and 12 km domains, every 20 minutes for the 4 km domain, and every 5 minutes for the 1 km domain. The WRF model was output at

higher temporal resolutions than hourly to prevent the output to be smoothed temporally. CMAQ was run to ingest the meteorology on the same temporal resolution as the WRF model output

WRF was run straight through (i.e., was not re-initialized at all) using an iterative technique developed at the EPA. The EPA successfully used the WRF iterative technique to simulate the meteorology and air quality during the DISCOVER-AQ Maryland field deployment. Like Houston, Maryland air quality is affected by local-scale bay breeze circulations. A description of improvements and benefits to the WRF-CMAQ system by the EPA, including a description of the WRF iterative technique, is described in Appel et al. (2014). The iterative technique involved running WRF twice. The first WRF run performed analysis nudging on all domains based on the 12 km NAM. The second WRF run performed analysis nudging on all domains based on the 12 km NAM except for 2 m temperature and humidity for the 4 and 1 km domains. 2 m temperature and humidity from 4 and 1 km 1st WRF iterative run was used to nudge the 2nd WRF iterative 4 and 1 km domains. This modeling technique prevented the relatively coarse NAM 12 km model from degrading the high resolution WRF modeling domains (4 and 1 km modeling domains). The 2nd iterative WRF runs were used to drive the improved CMAQ simulations.

For this project, the 4 km CMAQ was re-run for the month of September 2013 using the process analysis tool. The process analysis tool was used to output radical loss due to NOx (L_N), total primary radical production (Q), ozone production rate ($P(O_3)$), ozone loss rate ($L(O_3)$), and net ozone production rate (net $P(O_3)$). The fraction of radical loss due NOx (L_N/Q) is used to define VOC and NOx sensitive regimes ($L_N/Q > 0.5$: VOC limited; $L_N/Q < 0.5$: NOx limited).
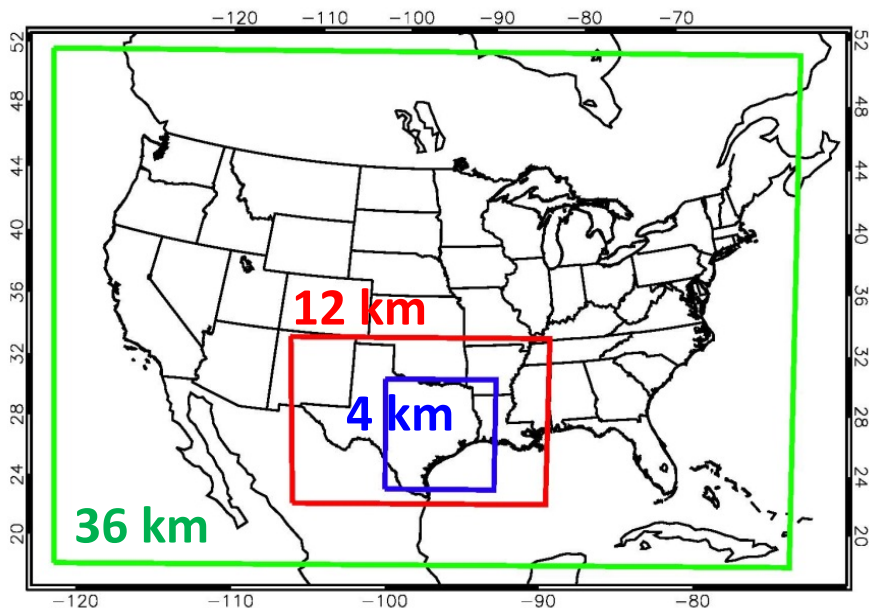
Figure 7-1. 36, 12, and 4 km CMAQ modeling domains.
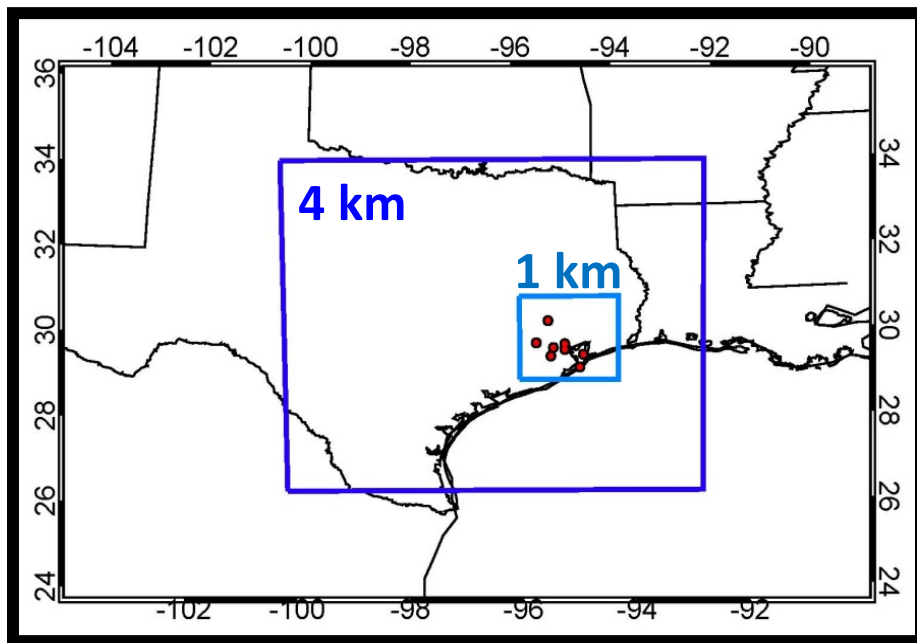
Figure 7-2. 4 and 1 km CMAQ modeling domains. The red dots show the NASA P-3B aircraft spiral locations.

Table 7-3. Terrain-following hydrostatic-pressure vertical coordinates (η) and the hydrostatic pressure (p_h) if surface pressure is 1013.25 mb for WRF and CMAQ simulations at the upper edge of each grid cell.

η	p_h	H	p_h	η	p_h	η	p_h
1	1013.25	0.8882	905.559	0.561	590.383	0.207792	250.156
0.9974	1010.75	0.8659	884.078	0.526963	557.597	0.18447	227.691
0.994	1007.47	0.841	860.093	0.492715	524.608	0.163354	207.351
0.99	1003.62	0.82069	840.53	0.458342	491.498	0.14	184.855
0.9854	999.187	0.79947	820.089	0.4242	458.611	0.12	165.59
0.9796	993.6	0.775938	797.422	0.390373	426.027	0.1	146.325
0.9723	986.568	0.750095	772.529	0.357176	394.05	0.083	129.95
0.9635	978.091	0.721941	745.41	0.324505	362.579	0.07	117.427
0.9528	967.785	0.691895	716.468	0.292674	331.918	0.052632	100.697
0.9401	955.551	0.660275	686.01	0.262209	302.573	0.03	78.8975
0.9252	941.199	0.627918	654.842	0.233845	275.251	0	50
0.9079	924.535	0.594721	622.865				

Table 7-4. WRF and CMAQ model options that were used in both the original and improved modeling scenarios.

Weather Research and Forecasting (WRF) Version 3.6.1 Model Options	
Radiation	Long Wave: Rapid Radiative Transfer Model (RRTM) Short Wave: Goddard
Surface Layer	Pleim-Xiu
Land Surface Model	Pleim-Xiu
Boundary Layer	Asymmetric Convective Model (ACM2)
Cumulus	Kain-Fritsch
Microphysics	WRF Single-Moment 6 (WSM-6)
Nudging	Observational and analysis nudging
Damping	Vertical velocity and gravity waves damped at top of modeling domain
SSTs	Multi-scale Ultra-high Resolution (MUR) SST analysis (~1 km resolution)
CMAQ Version 5.0.2 Model Options	
Chemical Mechanism	Carbon Bond (CB05)
Aerosol Module	Aerosols with aqueous extensions version 5 (AE5)
Dry deposition	M3DRY
Vertical diffusion	Asymmetric Convective Model 2 (ACM2)
Emissions	2012 TCEQ anthropogenic emissions Biogenic Emission Inventory System (BEIS) calculated within CMAQ
Initial and Boundary conditions	Model for OZone and Related chemical Tracers (MOZART) Chemical Transport Model (CTM)

The CMAQ model was run with process analysis to obtain ozone production ($P(O_3)$), higher oxides of nitrogen gases production ($P(NOz)$, hydrogen peroxide production ($P(H_2O_2)$), nitric acid production ($P(HNO3)$, and ozone production efficiency (OPE). The ratio of $P(H_2O_2)$ and $P(HNO_3)$ was used to determine which regions are NOx and VOC limited. The CMAQ modeling domains is slightly smaller than the WRF modeling domains (grid cells close to the horizontal edge of the WRF domains were be included in the CMAQ domains). WRF and CMAQ were evaluated with National Weather Service observations (meteorology), EPA's Air Quality System (AQS) observations (O_3 and particulate matter with particle diameters less than 2.5 micrometers ($PM_{2.5}$)), and final quality assured DISCOVER-AQ ground-, and aircraft-based observations of O_3, carbon monoxide (CO), oxides of nitrogen compounds (nitric oxide + nitrogen dioxide, NO_x) and NO_x plus all other higher oxides of nitrogen gases (NO_y), and ammonia (NH_3) as well as a suite of VOC species, and a suite of aerosols). DISCOVER-AQ data and descriptions of the data are available at http://www-air.larc.nasa.gov/missions/discover-aq/discover-aq.html. Curtain figures along the flight track of the P3 were created to compare model predictions with observations. The following statistics were calculated between the model results and observations to evaluate the model predictions and are shown in Table 1: mean bias, normalized

mean bias, normalized mean error, and root mean square error. Model-observation comparisons with the figures and statistics were analyzed to ascertain why model errors and uncertainties exist (i.e., errors in the emissions, chemistry, and/or transport processes). CMAQ model output was analyzed to map the OPE, NO_X limited areas, and VOC limited areas throughout the Houston metropolitan area. CMAQ model output was extracted for use in the box model.

Table 7-3. Definition of the statistics used in WRF and CMAQ model evaluations. In these equations M represents the model results, O represents the observations, and N is the number of data points.

Mean Bias (MB)	$$MB = \frac{1}{N}\sum_{i=1}^{N}(M_i - O_i)$$
Normalized Mean Bias (NMB)	$$NMB = \frac{\sum_{i=1}^{N}(M_i - O_i)}{\sum_{i=1}^{N}O_i} \times 100\%$$
Normalized Mean Error (NME)	$$NME = \frac{\sum_{i=1}^{N}|M_i - O_i|}{\sum_{i=1}^{N}O_i} \times 100\%$$
Root Mean-Square Error (RMSE)	$$RMSE = \sqrt{\frac{1}{N}\sum_{i=1}^{N}(M_i - O_i)^2}$$
Gross Error (G)	$$GE = \frac{1}{N}\sum_{i=1}^{N}|M_i - O_i|$$

An evaluation of the improved WRF and CMAQ model simulations for the entire month of September 2013 are displayed in this section. Statistics used to evaluate WRF and CMAQ are described Tables 7-3. Proposed benchmarks for evaluating WRF by Emery et al. (2001) are also shown in Table 7-4. The benchmarks were created to help put model results into context, not give them a passing or failing grade. For example, expectations for simulating the meteorology of a complex local-scale circulation, like sea and bay breeze circulations in and around Houston are not as high as simulating meteorology over flat terrain. CMAQ simulated a high bias in surface and aloft ozone (Tables 7-5). CMAQ also simulated a low bias in CO, CH_2O, isoprene, NO_2, and NO aloft and a high bias in NOy aloft (Table 7-6). Recent work has shown that oceanic emissions of iodine and bromine result in ozone destruction (Carpenter et al., 2013). The high ozone bias in our results is expected due to the lack of oceanic iodine and bromine emissions and the associated chemistry. Biases in surface ozone are larger near the coastline (i.e., Galveston) than sites inland (i.e., Conroe) as shown in Figure 7-3.

Table 7-4. Mean bias (MB), normalized mean bias (NMB), normalized mean error (NME), root mean square error (RMSE), and Gross Error (GE) of 2 m temperature, 10 m wind speed, and 10 m wind direction for the 2nd iterative 1 km WRF simulations covering all of September 2013.

	2 m Temperature (K)		10 m Wind Speed (m/s)		10 m Wind Direction (deg)	
	Bench mark	Model	Bench mark	Model	Bench mark	Model
MB	≤ ±0.5 K	0.2	≤ ±0.5 m/s	-0.8	≤ ±10°	32
NMB (%)		0.1		-17		26
NME (%)		0.4		36		26
RMSE		1.6	≤ 2 m/s	2.3		51
GE	≤ ± 2 K	1.2		1.7	≤ 30°	32

Table 7-5. Mean bias (MB), normalized mean bias (NMB), normalized mean error (NME), root mean square error (RMSE), and Gross Error (GE) of surface ozone for the 2nd iterative 1 km WRF simulations covering all of September 2013.

	Surface Ozone (ppbv)
MB	9.5
NMB (%)	39
NME (%)	51
RMSE	15
GE	12

Table 7-6. Second iterative 1 km CMAQ simulated mean bias (MB), normalized mean bias (NMB), normalized mean error (NME), and root mean square error (RMSE) of O_3, CO, CH_2O, Isoprene (ISO), NO_2, NO, and NOy covering measurements made onboard the NASA P-3B aircraft on all flight days during the DISCOVER-AQ field campaign

		O_3	CO	CH_2O	ISO	NO2	NO	NOy
Model	MB	0.8	-5.8	-0.3	-0.02	-0.5	-0.3	0.04
	NMB	1.4	-4.8	-16	-7.7	-39	-66	1.3
	NME	15	17	37	70	70	84	61
	RMSE	12	35	1.4	0.7	3.1	2.2	4.7
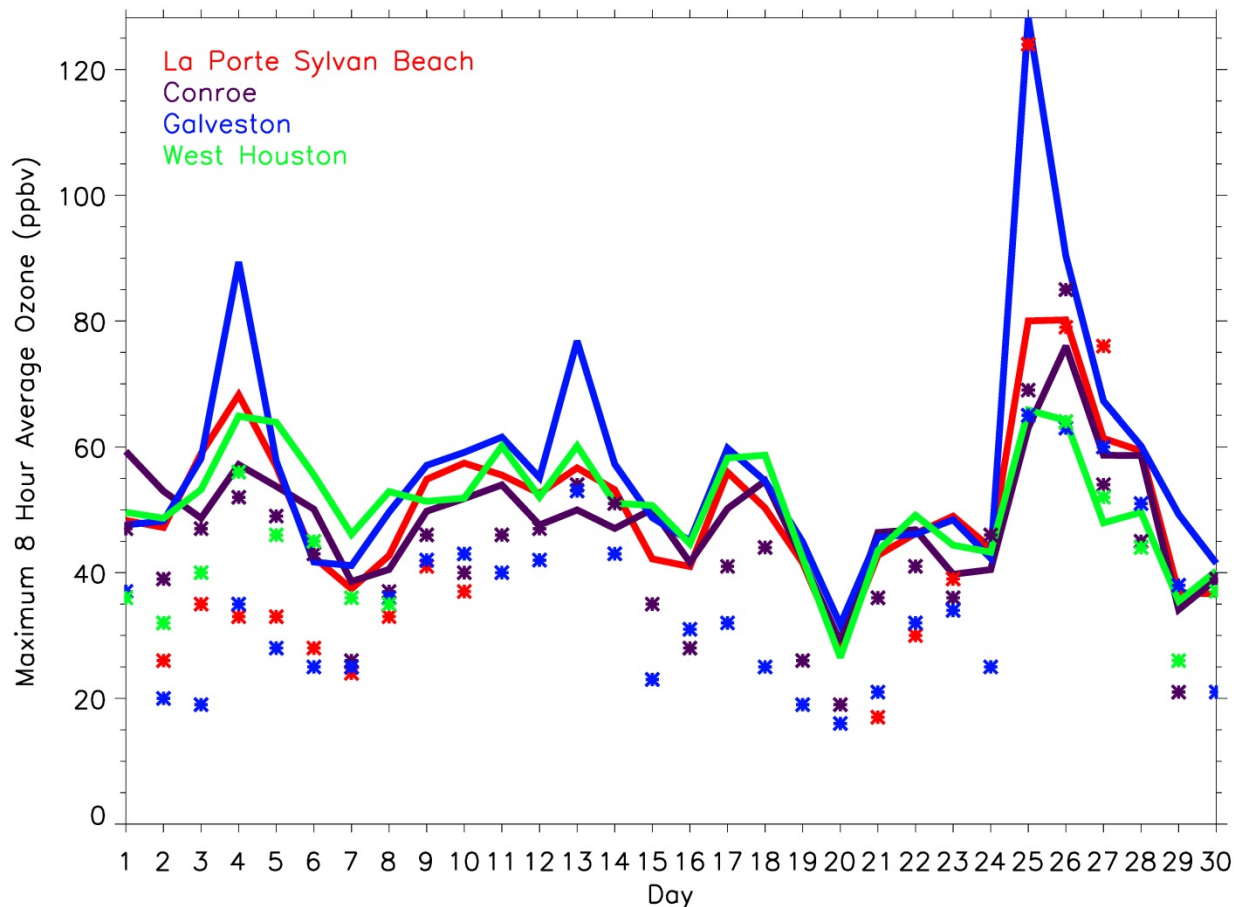
Figure 7-3. Observed (*) and CMAQ simulated (solid lines) maximum 8 hour average ozone at La Porte Sylvan Beach (red), Conroe (purple), Galveston (blue), and West Houston (green) during September 2013.

(2) Box Model Simulations

An observation-constrained box model with the Carbon Bond Mechanism Version 2005 (CB05) was used to simulate the oxidation processes in Houston during DISCOVER-AQ. Use of a box model is essential because it can quickly, in a matter of minutes, simulate environmental conditions. Measurements made on the P-3B and at the eight science sites were used as input to constrain the box model. Using the model results, the ozone production rate and its sensitivity to NO_x and VOCs were calculated. The model results also allow us to calculate ozone production efficiency at different locations and at different times of a day.

The Carbon Bond Mechanism Version 2005 (CB05) was used in box modeling for the data analysis in this project. This mechanism is well known and has been actively in use in research and regulatory applications [Yarwood et al., 2005; Goliff et al., 2013]. The original mechanism was used while kinetic data were updated based on the most recent chemical kinetic data evaluations [e.g., Sander et al, 2011; Atkinson et al., 2004; 2006; 2007; 2008]. The box model was constructed and run on the platform of FACSIMILE for Windows software (MCPA Software, Ltd), which has been successfully used in the modeling effort for previous research projects [e.g., Chen et al., 2010; Ren et al., 2013].

The Carbon Bond Mechanism (CB05) [Yarwood et al., 2005] is an updated version of CB4. In contrast to the previous version, (1) inorganic reactions are extended to simulate remote to polluted urban conditions; and (2) two extensions are available to be added to the core mechanism for modeling explicit species and reactive chlorine chemistry. Organic species are lumped according to the carbon bond approach, that is, bond type, e.g., carbon single bond and double bond. Reactions are aggregated based on the similarity of carbon bond structure so that fewer surrogate species are needed in the model. For instance, the single-bonded one-carbon-atom surrogate photosynthetically active radiation (PAR) represents alkanes and most of the alkyl groups. Some organics (e.g., organic nitrates and aromatics) are lumped in a similar manner as done in Regional Atmospheric Chemical Mechanism, Version 2 (RACM2).

In order to run the box model, measurements, including long-lived inorganic and organic compounds and meteorological parameters (temperature, pressure, humidity, and photolysis frequencies) measured on the NASA P-3B were averaged into 1-minute values that became the model input. For each data point, the model ran for 24 hours, long enough to allow most calculated reactive intermediates to reach steady state but short enough to prevent the buildup of secondary products. A deposition lifetime of two days was assumed for all calculated species to avoid unexpected accumulation of these species in the model. At the end of 24 hours, the model generated time series of OH, HO_2, RO_2, and other reactive intermediates with an interval of 1 minute. The box model covered the entire P-3B flight track during DISCOVER-AQ, including the eight science sites where the P-3B conducted spirals.

It is worth noting that unlike a three-dimensional chemical transport model, the zero-dimensional (box) model simulations did not include advection and emissions, although advection and emissions are certainly important factors for the air pollution formation. Because all of the long-lived radical precursors and O_3 precursors were measured and used to constrain the box model calculations, the advection and emissions can be neglected for this project of radicals and their production and loss rates.

During the day, the photochemical O_3 production rate is essentially the production rate of NO_2 molecules from $HO_2 + NO$ and $RO_2 + NO$ reactions [*Finlayson-Pitts and Pitts*, 2000]. The net instantaneous O_3 production rate, $P(O_3)$, can be written approximately as the following equation:

$$P(O_3) = k_{HO_2+NO}[HO_2][NO] + \sum k_{RO_{2i}+NO}[RO_{2i}][NO] - k_{OH+NO_2+M}[OH][NO_2][M] - P(RONO_2)$$
$$-k_{HO_2+O_3}[HO_2][O_3] - k_{OH+O_3}[OH][O_3] - k_{O(^1D)+H_2O}[O(^1D)][H_2O] - L(O_3 + alkenes) \qquad (1)$$

where, *k term*s are the reaction rate coefficients; RO_{2i} is the individual organic peroxy radicals; and $P(RONO_2)$ is the production rate of organic nitrates ($RONO_2$). The negative terms in Eq. (1) correspond to the reaction of OH and NO_2 to form nitric acid, the formation of organic nitrates, $P(RONO_2)$, the reactions of OH and HO_2 with O_3, the photolysis of O_3 followed by the reaction of $O(^1D)$ with H_2O, and O_3 reactions with alkenes.

The dependence of O_3 production on NOx and VOCs can be categorized into two typical scenarios: NO_x sensitive and VOC sensitive. The method proposed by *Kleinman* [2005b] was used to evaluate the O_3 production sensitivity using the ratio of L_N/Q, where L_N is the radical loss via the reactions with NO_x and Q is the total primary radical production. Because the radical production rate is approximately equal to the radical loss rate, this L_N/Q ratio represents the fraction of radical loss due to NO_x. It was found that when L_N/Q is significantly less than 0.5, the atmosphere is in a NO_x-sensitive regime, and when L_N/Q is significantly greater than 0.5, the atmosphere is in a VOC-sensitive regime [*Kleinman et al.*, 2001; *Kleinman*, 2005b]. Note that the contribution of organic nitrates impacts the cut-off value for L_N/Q to determine the ozone

production sensitivity to NO_x or VOCs and this value may vary slightly around 0.5 in different environments.

Using the box model simulation results, ozone production rates were calculated based on Eq. (1) and investigate the ozone production sensitivity to NO_x and VOCs along the NASA P-3B flight tracks during DISCOVER-AQ as well as at eight surface sites where the P-3B conducted spiral profiles (Figure 1). Spatial and temporal variations of ozone production and its sensitivity along the P-3B flight tracks and at the spiral sites were investigated in detail. Science questions listed in the Objectives Section above can then be answered.

10. APPENDIX D – INORGANIC AND ORGANIC SPECIES USED IN THE CB05 CHEMICAL MECHANISM

Table 8-1. Species names for the CB05 chemical mechanism

Species Name	Description	Number of Carbons
NO	Nitric oxide	0
NO2	Nitrogen dioxide	0
O3	Ozone	0
O	Oxygen atom in the $O^3(P)$ electronic state	0
O1D	Oxygen atom in the $O^1(D)$ electronic state	0
OH	Hydroxyl radical	0
HO2	Hydroperoxy radical	0
H2O2	Hydrogen peroxide	0
NO3	Nitrate radical	0
N2O5	Dinitrogen pentoxide	0
HONO	Nitrous acid	0
HNO3	Nitric acid	0
PNA	Peroxynitric acid (HNO_4)	0
CO	Carbon monoxide	1
FORM	Formaldehyde	1
ALD2	Acetaldehyde	2
C2O3	Acetylperoxy radical	2
PAN	Peroxyacetyl nitrate	2
ALDX	Propionaldehyde and higher aldehydes	2
CXO3	C3 and higher acylperoxy radicals	2
PANX	C3 and higher peroxyacyl nitrates	2
XO2	NO to NO2 conversion from alkylperoxy (RO_2) radical	0
XO2N	NO to organic nitrate conversion from alkylperoxy (RO_2) radical	0
NTR	Organic nitrate (RNO_3)	1
ETOH	Ethanol	2
CH4	Methane	1
MEO2	Methylperoxy radical	1
MEOH	Methanol	1
MEPX	Methylhydroperoxide	1
FACD	Formic acid	1
ETHA	Ethane	2
ROOH	Higher organic peroxide	1
AACD	Acetic and higher carboxylic acids	2
PACD	Peroxyacetic and higher peroxycarboxylic acids	2
PAR	Paraffin carbon bond (C-C)	1
ROR	Secondary alkoxy radical	0
ETH	Ethene	2
OLE	Terminal olefin carbon bond (R-C=C)	2
IOLE	Internal olefin carbon bond (R-C=C-R)	4
ISOP	Isoprene	5
ISPD	Isoprene product (lumped methacrolein, methyl vinyl ketone, etc.)	4
TERP	Terpene	10
TOL	Toluene and other monoalkyl aromatics	7
XYL	Xylene and other polyalkyl aromatics	8
CRES	Cresol and higher molecular weight phenols	8
TO2	Toluene-hydroxyl radical adduct	7
OPEN	Aromatic ring opening product	4
CRO	Methylphenoxy radical	7
MGLY	Methylglyoxal and other aromatic products	3
SO2	Sulfur dioxide	0
SULF	Sulfuric acid (gaseous)	0